

A General Model of Radial Dispersion with Wellbore Mixing and Skin Effects

Wenguang Shi¹, Quanrong Wang^{1,2,3*}, Hongbin Zhan⁴ and Renjie Zhou⁵

¹School of Environmental Studies, China University of Geosciences, 388 Lumo Road, Wuhan 430074, China

5 ²State Environmental Protection Key Laboratory of Source Apportionment and Control of Aquatic Pollution, Ministry of Ecology and Environment, Wuhan, Hubei 430074, PR China

³Hubei Key Laboratory of Yangtze River Basin Environmental Aquatic Science, School of Environmental Studies, China University of Geosciences, Wuhan, Hubei 430074, PR China

⁴Department of Geology and Geophysics, Texas A& M University, College Station, TX 77843-3115, USA

10 ⁵Department of Environmental and Geosciences, Sam Houston State University, Huntsville, TX 77340, USA

Correspondence to: Quanrong Wang (wangqr@cug.edu.cn)

Abstract.

The mechanism of radial dispersion is important for understanding reactive transport in the subsurface and for
15 estimating aquifer parameters required in the optimization design of remediation strategies. Many previous
studies demonstrated that injected solute firstly experienced a mixing process in the injection wellbore, then
entered a skin zone after leaving the injection wellbore, and finally moved into the aquifer through advective,
diffusive, dispersive, and chemical-biological-radiological processes. In this study, a physically-based new model
and associated analytical solutions in Laplace domain are developed by considering the mixing effect, skin effect,
20 scale effect, aquitard effect and media heterogeneity (in which the solute transport is described in a mobile-
immobile framework). This new model is tested against a finite-element numerical model and experimental data.
The results demonstrate that the new model performs better than previous models of radial dispersion in
interpreting the experimental data. To prioritize the influences of different parameters on the breakthrough curves,
a sensitivity analysis is conducted. The results show that the model is sensitive to the mobile porosity and
25 wellbore volume, and the sensitivity coefficient of wellbore volume increases with the well radius, while it
decreases with increasing distance from the wellbore. The new model represents the most recent advancement on
radial dispersion study that incorporates a host of important processes that are not taken into consideration in
previous investigations.

Keywords: Solute transport; Recharge well; Divergent flow; Parameter estimation; Push-and-pull test

1 Introduction

Radial dispersion refers to a process of reactive transport under the radial flow condition. One unique feature of radial dispersion (as compared to unilateral dispersion where the flow velocity is unilateral) is that the dispersive transport becomes progressively weaker when the radial distance from the injection/pumping well becomes larger (or the radial flow velocity becomes smaller), thus the relative importance of molecular diffusion (which is assumed to be constant) versus the dispersion becomes progressively stronger with larger radial distance. The radial dispersion problem is both theoretically interesting and practically important in many fields, like chemical engineering (Davis and Davis, 2002), environmental science (Reinhard et al., 1997), and hydrogeology (Webster et al., 1970). Although numerical modelling is probably inevitable and more powerful than the analytical modelling in describing radial dispersion, especially put forward for heterogeneous aquifers with complex initial and boundary conditions, the numerical errors and computational cost are not always trivial issues and have to be considered by the engineers. As an alternative, many analytical models have been developed for radial dispersion around an injection well under rather simplified conditions. Such analytical models can fulfil a host of tasks such as 1) prioritizing the importance of different controlling parameters through a sensitivity analysis; 2) benchmarking the numerical solutions to elucidate the possible numerical errors such as numerical dispersion and artificial oscillation which are notorious for advection-dominated transport problems; 3) providing a quick screening tool before implementing a full-scale comprehensive study.

Because of above-mentioned benefits, significant efforts have been put forward over many decades on developing advanced analytical models of radial dispersion. Some examples include the works of

Hoopes and Harleman (1967), Gelhar and Collins (1971), Tang and Babu (1979), Moench and Ogata (1981), Chen (1985), Chen (1986), Hsieh (1986), Tang and Peaceman (1987), Yates (1988), Falade and Brigham (1989), Chen (1991), Novakowski (1992), Philip (1994), Veling (2001), Huang and Goltz (2006), Chen et al. (2007), Gao et al. (2009a), Chen et al. (2011), Cihan and Tyner (2011), Veling (2011), Chen et al. (2012), Wang and Zhan (2013a), Hsieh and Yeh (2014), Zhou et al. (2017), [Chen et al. \(2017\)](#), Wang et al. (2018), [Huang et al. \(2019\)](#), [Li et al. \(2020\)](#), [Wang et al. \(2020\)](#) and so on. A general trend of such developments is to provide models that are more robust and can better represent the physical reality. However, despite the enormous efforts up to date, some significant pitfalls still exist and become roadblocks for quick and accurate interpretation of observed data in the experiments. A major task of this research is to eliminate such pitfalls which are briefly illustrated in the following.

In a well-aquifer system with radial dispersion, the region could be horizontally divided into three parts: wellbore, skin zone, and aquifer formation zone. The skin zone refers to the disturbed region around the well caused by drilling and construction practices or well completion (Yeh and Chang, 2013; Chen et al., 2012; [Li et al., 2020](#); [Li et al., 2019](#); [Huang et al., 2019](#)). [It is spatially between well screen and aquifer formation zone](#). Correspondingly, the injected solute may experience three processes from the wellbore to the aquifer formation zone.

Firstly, the injected solute goes through a mixing process with native (or pre-injection) water in the wellbore at the early stage of injection, which is called mixing effect. Probably due to the small radius of the well, the mixing effect has been overlooked by almost all the analytical solutions mentioned above except Novakowski (1992) ~~and~~, Wang et al. (2018), [Shi et al. \(2020\)](#) and [Wang et al. \(2020\)](#), e.g., either by assuming that the well radius was infinitesimal, or assuming that the solute concentration in

the wellbore was the same as the concentration of the injected solution (Hoopes and Harleman, 1967;Veling, 2011;Zhou et al., 2017). Consequently, the solutions developed without considering the wellbore mixing effect may overestimate concentration values in both the wellbore and the aquifer (Novakowski, 1992;Wang et al., 2018;[Shi et al., 2020](#); [Wang et al., 2020](#)). The reason is that the solute concentration in the wellbore is initially zero (when the aquifer is free of solute before the injection), and then increases steadily until it is up to the maximum, which is equal to the concentration of the injected solution.

Secondly, the solute enters the skin zone after leaving the wellbore. [Comparing with aquifer formation zone of interest, the dimension of the skin zone is much smaller, e.g., ranging from 0.1 m to several meters, and it is ignored or included in wellbore. In another word, the effect of the skin zone on radial dispersion \(named as skin effect\) was negligible. However, numerous previous studies demonstrated that the existence of a skin zone might significantly alter the mechanism of groundwater flow and solute transport around well \(Chen et al., 2012;Hsieh and Yeh, 2014;Yeh and Chang, 2013; Li et al., 2020;Li et al., 2019\). Although the dimension of the skin zone might be very small, e.g., ranging from 0.1 m to several meters, numerous previous studies demonstrated that the existence of a skin zone might significantly alter the mechanism of groundwater flow and solute transport \(Chen et al., 2012;Hsieh and Yeh, 2014;Yeh and Chang, 2013;\).](#) This is because the physical properties (such as permeability, porosity, dispersivity, and so on) of the skin zone are often vastly different from their counterparts of the formation zone. Previously, studies on the skin effect were mainly concentrated on the groundwater flow process around the well, and much less attention was paid to solute transport processes. [To date, few studies considered the skin effect among the above-mentioned analytical models on radial](#)

dispersionFor instance, such as Chen et al. (2012)~~and~~, Hsieh and Yeh (2014), Huang et al. (2019) and
95 Li et al. (2020)are probably the only two studies considering the skin effect among the above-mentioned
analytical models on radial dispersion. Chen et al. (2012) proposed an analytical solution of solute
transport with skin effect to investigate the influences of dispersivity on radial dispersion, soon after,
Hsieh and Yeh (2014) extended the model of Chen et al. (2012) by taking into account a third-type
(Robin) condition. Huang et al. (2019) demonstrated that the skin effect has a major influence on
100 observed breakthrough curves (BTCs) for radially convergent tracer tests. Recently, Li et al. (2020)
developed the analytical model for radial reactive transport with skin effect to investigate the impacts of
dispersivity, effective porosity and mass transfer coefficient in skin zone on radial dispersion. The
above-mentioned studies demonstrated the skin effects are significant for radial dispersion.

Thirdly, the solute moves into the formation zone from the skin zone by advective, diffusive, and
105 dispersive processes. Such processes have been widely described by the traditional advection-dispersion
equation (ADE) which is based on Fick's law; however, many recent studies demonstrated that the
ADE model mainly worked well for homogeneous (or nearly homogeneous) porous media. As for
reactive transport in heterogeneous media, the ~~observed breakthrough curves (BTCs)~~ may exhibit a host
of non-Fickian characteristics such as early arrival and heavy tailing (Di Dato et al., 2017;Molinari et al.,
110 2015). Alternatively, many non-Fickian transport models have been developed, such as the multi-rate
mass transfer model (MRMT) (Le Borgne and Gouze, 2008;Haggerty et al., 2001), mobile-immobile
model (MIM) (van Genuchten and Wierenga, 1976;Zhou et al., 2017;Wang et al., 2020), continuous-
time random-walk models (CTRW) (Dentz et al., 2015;Hansen et al., 2016), fractional-derivative ADE
models (fADE) (Soltanpour Moghadam et al., 2022;Chen et al., 2017), a combination of MRMT and

115 CTRW (Kang et al., 2015), and so on (Zheng et al., 2019;Lu et al., 2018). Although the models of
MRMT, CTRW and fADE perform well in modeling non-Fickian transport, it is not easy to obtain the
analytical solutions of these models. Meanwhile, these theories are usually not easy to apply for solving
regional-scale transport problems, as pointed out in a recent study (Zheng et al., 2019). MIM is an
extension of ADE by considering both flowing and stagnant regions in porous media and mass transfer
120 between them (van Genuchten and Wierenga, 1976;Zhou et al., 2017;Wang et al., 2020), ~~and~~ Zhou et al.
(2017) and Wang et al. (2020) derived the MIM solutions ~~associated with~~ radial dispersion. However,
the skin effect and the scale effect were ignored in their studies, which will be investigated in this
study. ~~Meanwhile, these theories are usually not easy to apply for solving regional scale transport~~
~~problems, as pointed out in a recent study (Zheng et al., 2019).~~ Besides the MRMT, MIM, CTRW, and
125 fADE models, another approach to represent the heterogeneity is to use a scale-dependent dispersivity
(or dispersion) in the ADE or MIM models (Haddad et al., 2015;Gelhar et al., 1992). Gao et al. (2009a)
and Chen et al. (2007) discussed radial dispersion and found that the scale-dependent dispersion effect
was not negligible. There are also experimental evidence for the scaling of dispersion, mixing, and
reaction (Leitão et al., 1996;Edery et al., 2015).
130 The differences among the currently available analytical solutions for radial dispersion have been
reviewed and summarized in Table 1. As one can see from this table, the mixing effect in the wellbore
was ignored in all of the models except for Novakowski (1992)~~and~~, Wang et al. (2018), Shi et al. (2020)
and Wang et al. (2020). Only Chen et al. (2012)~~and~~, Hsieh and Yeh (2014), Huang et al. (2019) and Li
et al. (2020) took the skin effect into account. The differences among the solutions of Tang and Babu
135 (1979), Moench and Ogata (1981), Hsieh (1986), Tang and Peaceman (1987), Yates (1988), Cihan and

Tyner (2011), and Chen et al. (2012a) mainly consist in the boundary conditions, source-injection types (instantaneous or continuous), and initial conditions.

In summary, no existing analytical model has ever considered the mixing effect, skin effect, scale effect and media heterogeneity effect (which is described using MIM) simultaneously. Although the numerical method is more powerful than the analytical method for problems with complex initial and boundary conditions and heterogeneous aquifers of interest, numerical errors could not be avoided easily for the MIM models of concern here, such as numerical dispersion and numerical oscillation issues (Zheng and Wang, 1999; Wang and Zhan, 2013b). Meanwhile, the analytical solutions are usually computationally more efficient than the numerical solutions, and can be easily coupled into optimization algorithms for problems related to parameter estimation (Neuman and Mishra, 2012). Therefore, a primary purpose of this study is to develop such an analytical model. Furthermore, the accuracy and robustness of the developed model will be tested against a finite-element numerical simulation and experimental data. Moreover, a sensitivity analysis will be conducted to prioritize the influences of various controlling parameters on the newly developed radial dispersion reactive transport model.

2 Methods

2.1 Mathematical model of radial dispersion

An aquifer is assumed to be confined, homogeneous, horizontally isotropic, with a constant thickness, and fully penetrated by a well from which the solute is injected. A cylindrical coordinate system is established with the r -axis horizontal and the z -axis vertically upward. The origin of the coordinate

155 system is located at intersect of the well center and the middle elevation of the aquifer. A schematic diagram of the problem is available in Figure S1 of *Supplementary Materials*.

In this study, we mainly focus on developing analytical solutions of radial dispersion with a Heaviside step source (or step function for abbreviation hereinafter), as solutions of a variety of injection scenarios can be easily obtained on the basis of such a step source solution, as shown in Eq. (A2) in
 160 *Supplementary Materials*, Eqs. (4a) - (4b), or Eqs. (5a) - (5b). Assuming that t_{inj} is the duration of the step source, the solute source concentration (C_0) is $C_{inj}(t)$ ~~nonzero~~ when time is smaller than t_{inj} , while it is $C_{cha}(t)$ ~~zero~~ when time is greater than t_{inj} , in which $C_{inj}(t)$ and $C_{cha}(t)$ represent the solute concentrations $[ML^{-3}]$ in the wellbore before time t_{inj} and after time t_{inj} , respectively; When $C_{cha}(t) = 0$. ~~The flow rate is constant in the entire time smaller than t_{inj} . When and~~ t_{inj} approaches
 165 zero but the total injected mass remains finite, the model of the step source reduces to the model of the instantaneous injection. Similarly, the model of the step source becomes the model of the continuous injection source when t_{inj} becomes infinity.

Similar to Chen et al. (2012) and Hsieh and Yeh (2014), a two-region (skin and formation) model of radial dispersion is employed to describe the skin effect. In the skin zone, the governing equations of
 170 radial dispersion are

$$\theta_{m1} R_{m1} \frac{\partial C_{m1}}{\partial t} = \frac{\theta_{m1}}{r} \frac{\partial}{\partial r} \left(r \alpha_1 |v_{a1}| \frac{\partial C_{m1}}{\partial r} \right) - \theta_{m1} v_{a1} \frac{\partial C_{m1}}{\partial r} - \omega_1 (C_{m1} - C_{im1}) - \theta_{m1} \mu_{m1} C_{m1}, r_w \leq r \leq r_s, \quad (1a)$$

$$\theta_{im1} R_{im1} \frac{\partial C_{im1}}{\partial t} = \omega_1 (C_{m1} - C_{im1}) - \theta_{im1} \mu_{im1} C_{im1}, r_w \leq r \leq r_s; \quad (1b)$$

In the formation zone, one has

$$\theta_{m2}R_{m2}\frac{\partial C_{m2}}{\partial t} = \frac{\theta_{m2}}{r}\frac{\partial}{\partial r}\left(r\alpha_2|v_{a2}|\frac{\partial C_{m2}}{\partial r}\right) - \theta_{m2}v_{a2}\frac{\partial C_{m2}}{\partial r} - \omega_2(C_{m2} - C_{im2}) - \theta_{m2}\mu_{m2}C_{m2}, r > r_s, (1c)$$

$$175 \quad \theta_{im2}R_{im2}\frac{\partial C_{im2}}{\partial t} = \omega_2(C_{m2} - C_{im2}) - \theta_{im2}\mu_{im2}C_{im2}, r > r_s, \quad (1d)$$

where the subscripts “ m ” and “ im ” refer to parameters in the mobile and immobile domains, respectively; the subscripts “1” and “2” refer to parameters in the skin and formation regions, respectively; C_{m1} and C_{im1} are the mobile and immobile concentrations [ML^{-3}] of the skin zone, respectively; C_{m2} and C_{im2} are the mobile and immobile concentrations [ML^{-3}] of the formation zone, respectively; r is the radial distance [L] from the center of the well; r_w is the well radius; r_s is the radial distance [L] from the center of the well to the outer boundary of the skin zone; v_a is the average radial pore velocity [LT^{-1}] in the aquifer; $v_{a1} = \frac{u_{a1}}{\theta_{m1}}$; $v_{a2} = \frac{u_{a2}}{\theta_{m2}}$; u_{a1} and u_{a2} represent Darcian velocities [LT^{-1}] in the skin and formation zones, respectively; α_1 and α_2 represent the longitudinal dispersivities [L] in the skin and formation zones, respectively; μ_{m1} , μ_{im1} , μ_{m2} and μ_{im2} are reaction rates for the first-order reaction rate, or the first-order biodegradation, or the radioactive decay [T^{-1}]; θ_{m1} , θ_{im1} , θ_{m2} and θ_{im2} are porosities; R_{m1} , R_{im1} , R_{m2} and R_{im2} are retardation factors [dimensionless]; ω_1 and ω_2 represent the first-order mass transfer coefficients [T^{-1}] between the mobile and immobile dissolved phases in the skin and formation zones, respectively. One point to note is that the molecular diffusive effect is assumed to be negligible in above governing equations.

190 Assuming that the skin and formation zone are initially free of solute, the initial conditions are

$$C_{m1}(r, t)|_{t=0} = C_{im1}(r, t)|_{t=0} = C_{m2}(r, t)|_{t=0} = C_{im2}(r, t)|_{t=0} = 0, r \geq r_w. \quad (2)$$

The outer boundary condition at an infinite distance is

$$C_{m2}(r, t)|_{r \rightarrow \infty} = C_{im2}(r, t)|_{r \rightarrow \infty} = 0. \quad (3)$$

Two types of models have been widely applied to the boundary condition at the well screen: the mass
 195 flux continuity (MFC) model and the resident concentration continuity (RCC) model. The RCC model is

$$[C_{m1}(r, t)]|_{r=r_w} = [C_{inj}(t)]|_{r=r_w}, 0 < t \leq t_{inj}, \quad (4a)$$

$$[C_{m1}(r, t)]|_{r=r_w} = [C_{cha}(t)]|_{r=r_w}, t > t_{inj}, \quad (4b)$$

and the MFC model is

$$\left[C_{m1}(r, t) - \alpha_1 \frac{|v_{a1, inj}|}{v_{a1, inj}} \frac{\partial C_{m1}(r, t)}{\partial r} \right] \bigg|_{r=r_w} = [C_{inj}(t)]|_{r=r_w}, 0 < t \leq t_{inj}, \quad (5a)$$

$$200 \quad \left[C_{m1}(r, t) - \alpha_1 \frac{|v_{a1, cha}|}{v_{a1, cha}} \frac{\partial C_{m1}(r, t)}{\partial r} \right] \bigg|_{r=r_w} = [C_{cha}(t)]|_{r=r_w}, t > t_{inj}, \quad (5b)$$

where ~~$C_{inj}(t)$ and $C_{cha}(t)$ represent the solute concentrations $[ML^{-3}]$ in the wellbore before time t_{inj}~~

~~and after time t_{inj} , respectively;~~ $v_{a1, inj}$ and $v_{a1, cha}$ refer to velocities in the injection and chasing

phases, respectively. It was demonstrated that the mass balance requirement could not be satisfied in the

RCC model, while the resident concentration was not continuous in the MFC model (Wang et al. 2018).

205 Many experimental studies demonstrated that the MFC model performed better than the RCC model

(Novakowski, 1992a). Therefore, the MFC model will be used to describe the boundary condition in the

wellbore in this study. Comparing Eqs. (4) and (5), one may find that the main difference between these

two models is whether the dispersivity is involved or not. Recently, Wang et al. (2019) pointed out that

the conflicts between these two models could be resolved by a scale-dependent dispersivity, which was

210 zero at the well screen, and increased with the travel distance of solute. This is because when the

dispersivity is zero in Eqs. (5a) - (5b), the MFC model reduces to the RCC model. The model of the scale-dependent dispersivity will be discussed in Section 2.4.

When taking into account the mixing effect in the wellbore, one has

$$V_{w,inj} \frac{dC_{inj}}{dt} = -\xi v_{a1,inj}(r_w)[C_{inj}(t) - C_0], 0 < t \leq t_{inj}, \quad (6)$$

$$215 \quad V_{w,cha} \frac{dC_{cha}}{dt} = -\xi v_{a1,cha}(r_w)[C_{cha}(t)], t > t_{inj}, \quad (7)$$

where $V_{w,inj}$ is the volume [L³] of water in the wellbore when $t \leq t_{inj}$, and $V_{w,inj} = \pi r_w^2 h_{w,inj}$; $h_{w,inj}$ is the water level [L] in the wellbore when $t \leq t_{inj}$; $\xi = 2\pi r_w \theta_{m1} B$; B is thickness [L] of aquifer; $V_{w,cha}$ is the volume [L³] of water in the wellbore when $t > t_{inj}$, and $V_{w,cha} = \pi r_w^2 h_{w,cha}$; $h_{w,cha}$ is the water level [L] in the wellbore when $t > t_{inj}$; $v_{a1,inj}(r_w)$ is velocity at the well screen in
 220 the injection phase, and $v_{a1,inj}(r_w) = \frac{Q_{inj}}{2\pi B r_w \theta_{m1}}$; $v_{a1,cha}(r_w)$ is velocity at the well screen in the chasing phase, and it equals to $\frac{Q_{cha}}{2\pi B r_w \theta_{m1}}$; Q_{inj} and Q_{cha} are the well flow rates [L³T⁻¹] in the injection and chasing phases, respectively. The mass balance for the well in Eqs. (6) -(7) is only relevant when velocity is greater than zero, because it does not contain terms for possible diffusive losses.

The water level in the wellbore (e.g., $h_{w,inj}$ and $h_{w,cha}$) could be determined by solving the
 225 groundwater flow model. In the steady state, one has

$$Q_{inj} = 2\pi r B K \frac{dh}{dr}, 0 < t \leq t_{inj}, \quad (8)$$

$$Q_{cha} = 2\pi r B K \frac{dh}{dr}, t > t_{inj}, \quad (9)$$

where K is the hydraulic conductivity [LT^{-1}], and $K = \begin{cases} K_1 & \text{when } r_w \leq r < r_s \\ K_2 & \text{when } r_s \leq r \end{cases}$; K_1 and K_2 are the hydraulic conductivities [LT^{-1}] of skin and formation zones, respectively.

230 By respectively conducting the integration on Eq. (8) and Eq. (9) from r_w to r_s and from r_s to r_e , the water level in the wellbore could be obtained as follows

$$h_{w,inj} = h_0 + \frac{Q_{inj}}{2\pi BK_1} \ln \frac{r_s}{r_w} + \frac{Q_{inj}}{2\pi BK_2} \ln \frac{r_e}{r_s}, 0 < t \leq t_{inj}, \quad (10)$$

$$h_{w,cha} = h_0 + \frac{Q_{cha}}{2\pi BK_1} \ln \frac{r_s}{r_w} + \frac{Q_{cha}}{2\pi BK_2} \ln \frac{r_e}{r_s}, t > t_{inj}, \quad (11)$$

where r_e is the radial distance [L] from the center of the well to the outer boundary of the formation zone; h_0 is hydraulic head [L] at r_e . One could find that a finite radius r_e is needed to keep h_w finite. It seems contradicts with the boundary condition of the transport problems, which is at the infinity as shown in Eq. (3). The reason for such a “contradiction” could be explained as follows. In reality, the influence area is limited by the finite injection rate and the finite injection time of the well (from a plane view perspective), bounded by a circle with a radius of r_e where the hydraulic head is almost constant
240 and the flow velocity is almost zero.

At the interface between the skin and formation zones, the concentration and dispersive flux have to be continuous, and one has

$$C_{m1}(r_s, t) = C_{m2}(r_s, t), t > 0, \quad (12)$$

$$\left[\alpha_1 |v_{a1}| \frac{\partial C_{m1}(r, t)}{\partial r} \right] \Big|_{r=r_s} = \left[\alpha_2 |v_{a2}| \frac{\partial C_{m2}(r, t)}{\partial r} \right] \Big|_{r=r_s}, t > 0. \quad (13)$$

245 Since Darcy fluxes (advective solute fluxes) are continuous, it follows that dispersive fluxes have to be continuous, which is Eq. (13).

Here, it is worthwhile to comment on the nature of using the MIM approach to describe transport in heterogeneous aquifers. First, it has been commonly observed that the aquifer heterogeneity renders the use of ADE invalid in many cases as ADE is developed and used primarily for homogeneous aquifers.

250 In particular, ADE fails to explain the early breakthrough and long tailing phenomena that are frequently observed in transport in heterogeneous aquifers, as illustrated in the introduction. Second, a striking feature of a heterogeneous aquifer is that a sequence of mobile and less mobile regions co-exist while a homogeneous aquifer may be simplified as a single (mobile) region. Ideally, if one knows exactly the spatial distribution of those mobile and less mobile regions and their associated flow and

255 transport parameters, one will be able to use a high-resolution numerical simulator to predict the flow and transport process precisely. Unfortunately, this is not feasible for most practical cases. Therefore, as an alternative, we have adopted the concept of MIM approach in which two continuums consisting of a mobile domain and an immobile domain co-exist over the entire heterogeneous aquifer. Each of these two continuums itself has uniform flow and transport parameters (such as porosity, retardation factor,

260 etc.) for the sake of simplification. Furthermore, mass can transfer between these two continuums in a certain fashion, usually using the first-order rate-limited equation. Third, this alternative approach has successfully explained a number of phenomena that cannot be explained using ADE, for instance, the early breakthrough and long tailing issues. Later on, the two-continuum MIM approach has been expanded to multiple-continuum MIM approach, or namely the multi-rate MIM approach to even better

265 capture the transport features in a heterogeneous aquifer (Vangenuchten and Wierenga, 1976;Elenius

and Abriola, 2019). In summary, the use of MIM is not to incorporate the spatial variation of flow and transport parameters that are mostly unknown. Instead, it is based on an alternative approach, using two or more interrelated continuums, and in each continuum the flow and transport parameters remain uniform over space. To date, the validation of the MIM model has been tested by numerous
270 experimental studies (Griffioen et al., 1998; Gao et al., 2009b; Elenius and Abriola, 2019).

2.2 Solution of radial dispersion

In this study, dimensionless forms of parameters used in the derivation of analytical solution are defined

$$\text{as: } C_{m1D} = \frac{C_{m1}}{C_0}, C_{im1D} = \frac{C_{im1}}{C_0}, C_{m2D} = \frac{C_{m2}}{C_0}, C_{im2D} = \frac{C_{im2}}{C_0}, C_{inj,D} = \frac{C_{inj}}{C_0}, C_{cha,D} = \frac{C_{cha}}{C_0}, t_D = \frac{|A|t}{\alpha_2^2 R_{m1}},$$

$$t_{inj,D} = \frac{|A|t_{inj}}{\alpha_2^2 R_{m1}}, r_D = \frac{r}{\alpha_2}, r_{wD} = \frac{r_w}{\alpha_2}, r_{sD} = \frac{r_s}{\alpha_2}, r_{0D} = \frac{r_0}{\alpha_2}, \mu_{m1D} = \frac{\alpha_2^2 \mu_{m1}}{A}, \mu_{im1D} = \frac{\alpha_2^2 R_{m1} \mu_{im1}}{R_{im1} A}, \mu_{m2D} =$$

$$275 \frac{\alpha_2^2 \mu_{m2} R_{m1}}{A R_{m2}}, \mu_{im2D} = \frac{\alpha_2^2 R_{m1} \mu_{im2}}{R_{im2} A} \text{ and } A = \frac{Q}{2\pi B \theta_{m1}}.$$

The detailed derivation of the analytical solution in the Laplace domain could be seen in Section S1 of *Supplementary Materials*. The analytical solution is

$$\bar{C}_{m1D} = N_1 \exp\left(\frac{r_D}{2\lambda}\right) A_i(y_1) + N_2 \exp\left(\frac{r_D}{2\lambda}\right) B_i(y_1), r_{wD} \leq r_D \leq r_{sD}, \quad (14a)$$

$$\bar{C}_{im1D} = \frac{\varepsilon_{im1}}{s + \varepsilon_{im1} + \mu_{im1D}} \bar{C}_{m1D}, r_{wD} \leq r_D \leq r_{sD}, \quad (14b)$$

$$280 \quad \bar{C}_{m2D} = N_3 \exp\left(\frac{r_D}{2}\right) A_i(y_2), r_D > r_{sD}, \quad (15a)$$

$$\bar{C}_{im2D} = \frac{\varepsilon_{im2}}{s + \varepsilon_{im2} + \mu_{im2D}} \bar{C}_{m2D}, r_D > r_{sD}, \quad (15b)$$

where $A_i(\cdot)$ and $B_i(\cdot)$ are the Airy functions of the first kind and second kind, respectively; $C_{inj,D}$ and $C_{cha,D}$ could be determined by Eqs. (A18) - (A19), which can be seen in Section S1 of *Supplementary Materials*; $A'_i(\cdot)$ and $B'_i(\cdot)$ are the derivatives of the Airy function of the first kind and second kind,

285 respectively; $\lambda = \frac{\alpha_1}{\alpha_2}$, $\eta = \frac{\theta_{m1}R_{m1}}{\theta_{m2}R_{m2}}$, $y_1 = \left(\frac{E_1}{\lambda}\right)^{1/3} \left(r_D + \frac{1}{4\lambda E_1}\right)$, $y_{1s} = \left(\frac{E_1}{\lambda}\right)^{1/3} \left(r_{sD} + \frac{1}{4\lambda E_1}\right)$, $y_2 = (E_2)^{1/3} \left(r_D + \frac{1}{4E_2}\right)$, $y_{2s} = (E_2)^{1/3} \left(r_{sD} + \frac{1}{4E_2}\right)$, $E_1 = s + \varepsilon_{m1} + \mu_{m1D} - \frac{\varepsilon_{m1}\varepsilon_{im1}}{s+\varepsilon_{im1}+\mu_{im1D}}$, $E_2 = \frac{1}{\eta} \left(s + \varepsilon_{m2} + \mu_{m2D} - \frac{\varepsilon_{m2}\varepsilon_{im2}}{s+\varepsilon_{im2}+\mu_{im2D}}\right)$, $\beta_{inj} = \frac{V_{w,inj}r_{wD}}{\xi R_{m1}\alpha_2}$, $\beta_{cha} = \frac{V_{w,cha}r_{wD}}{\xi R_{m1}\alpha_2}$, $\varepsilon_{m1} = \frac{\omega_1\alpha_2^2}{A\theta_{m1}}$, $\varepsilon_{im1} = \frac{\omega_1\alpha_2^2 R_{m1}}{A\theta_{im1}R_{im1}}$,

$\varepsilon_{m2} = \frac{\omega_2\alpha_2^2 R_{m1}}{A\theta_{m2}R_{m2}}$ and $\varepsilon_{im2} = \frac{\omega_2\alpha_2^2 R_{m1}}{A\theta_{im2}R_{im2}}$; s is the dimensionless Laplace transform parameter in respect to

dimensionless time t_D . the expressions for N_1 , N_2 and N_3 are listed in Table 2.

290 From Eqs. (14) - (15), one may find that it is not easy to analytically invert the Laplace-domain solution to obtain the real-time solution. Alternatively, numerical Laplace transform techniques such as the Fourier series method [\(Dubner and Abate, 1968\)](#), Zakian method [\(Zakian, 1969\)](#), Schapery method [\(Schapery, 1962\)](#), de Hoog method [\(De Hoog et al., 1982\)](#), Stehfest method [\(Stehfest and Harald, 1970\)](#) are called in, where the de Hoog and Stehfest methods perform better for problems related to radial dispersion (Wang and Zhan, 2015). In this study, the de Hoog method will be employed to conduct the inverse Laplace transform.

2.3. Special cases of the new solution

The new solution of this study considers the mixing effect, skin effect, and media heterogeneity (which is described using MIM) simultaneously, and the solute is injected into the well as a step source. This general solution encompasses many previous studies as special cases. For instance, when “ $r_s \rightarrow \infty$ ”, the

300

skin effect is excluded; “ $t_{inj} \rightarrow \infty$ ” implies that the solute is continuously injected into the well; while “ $t_{inj} \rightarrow 0$ ” means that the solute is instantaneously injected into the well; “ $\omega = 0$ ” implies that the MIM solution reduces to the ADE solution; “ $V_{w,inj} = 0$ ” or “ $r_w = 0$ ” shows that the mixing effect is excluded.

305 Therefore, the new solution reduces to the solutions of Hoopes and Harleman (1967), Gelhar and Collins (1971), Tang and Babu (1979), Moench and Ogata (1981), Hsieh (1986), Tang and Peaceman (1987), and Philip (1994) when $r_s \rightarrow \infty$, $t_{inj} \rightarrow \infty$, $\omega = 0$, and $V_{w,inj} = 0$. The solution of Wang et al. (2018) is a special case of this study when $r_s \rightarrow \infty$, $t_{inj} \rightarrow \infty$, and $\omega = 0$.

2.4. Extension of the new solution with scale-dependent dispersivity

310 Due to the heterogeneities of the porous media, the dispersivity was found to be dependent on travel distance of solute from source, and such phenomenon was firstly observed in the field scale experiment (Dagan, 1988;Gelhar et al., 1992;Pickens and Grisak, 1981a). The field scale effect (i.e., dispersivity growing with distance from well), is usually considered to be a result of spatial heterogeneity at different scales in the aquifer. Subsequently, the scale-dependent dispersivity phenomenon was also
315 found in controlled laboratory tests, due to heterogeneities caused by the bridging effect and microstructures, although the sediments (as the porous media) are well sorted and carefully packed (Silliman and Simpson, 1987;Berkowitz et al., 2000;Wang et al., 2019;Gao et al., 2010). For example, Silliman and Simpson (1987) found that the dispersivity continuously increased with distance, based on the experiments conducted in a $2.4 \times 1.07 \times 0.10$ m sandbox. Berkowitz et al. (2000) obtained similar
320 conclusions to Silliman and Simpson (1987) in the laboratory-controlled experiment. Wang et al. (2019)

also concluded that the scale-dependent model performed better than the scale-independent model in interpreting observed BTCs of the laboratory-controlled experiment. To date, four types of functions have been widely used to describe the scale-dependent dispersivity, including asymptotic, parabolic, exponential and linear functions, as summarized by Pickens and Grisak (1981b). In this section, the
 325 model of the scale-independent dispersivity (e.g., Eqs. (14) - (15) in Section 2) will be extended by considering the linear-asymptotic dispersivity model in the formation zone. As for the other types of scale-dependent functions, the analytical solutions could be derived using a similar approach. The formula of the linear distance-dependent dispersivity is

$$\alpha_2(r) = \begin{cases} kr, & r_s \leq r \leq r_0 \\ \alpha_0, & r > r_0 \end{cases}, \quad (16)$$

330 where r_0 is the distance [L] where $\alpha_2(r_0) = \alpha_0$, k is a constant [dimensionless], and the modified solutions are

$$\bar{C}_{m1D} = \mathcal{J}_1 \exp\left(\frac{r_D}{2\lambda}\right) A_i(y_1) + \mathcal{J}_2 \exp\left(\frac{r_D}{2\lambda}\right) B_i(y_1), r_{wD} \leq r_D \leq r_{sD}, \quad (17a)$$

$$\bar{C}_{im1D} = \frac{\varepsilon_{im1}}{s + \varepsilon_{im1} + \mu_{im1D}} \bar{C}_{m1D}, r_{wD} \leq r_D \leq r_{sD}, \quad (17b)$$

$$\bar{C}_{m2D} = \mathcal{J}_3 r_D^m K_m(\varepsilon_1 r_D) + \mathcal{J}_4 r_D^m I_m(\varepsilon_1 r_D), r_{sD} \leq r_D \leq r_{0D}, \quad (18a)$$

$$335 \quad \bar{C}_{m2D} = \mathcal{J}_5 \exp\left(\frac{r_D}{2}\right) A_i(y_3) + \mathcal{J}_6 \exp\left(\frac{r_D}{2}\right) B_i(y_3), r_D > r_{0D}, \quad (18b)$$

$$\bar{C}_{im2D} = \frac{\varepsilon_{im2}}{s + \varepsilon_{im2} + \mu_{im2D}} \bar{C}_{m2D}, r_D > r_{sD}, \quad (18c)$$

where $m = \frac{1}{2k}$; $K_m(\cdot)$ is m^{th} -order modified Bessel function of the second kind, $I_m(\cdot)$ is m^{th} -order modified Bessel function of the first kind; the expressions for $\mathcal{J}_1, \mathcal{J}_2, \mathcal{J}_3, \mathcal{J}_4, \mathcal{J}_5$ and \mathcal{J}_6 are listed in Table

3; $y_3 = (\varepsilon_1)^{1/3} \left(r_D + \frac{1}{4\varepsilon_1} \right)$; $y_4 = (\varepsilon_1)^{1/3} \left(r_{0D} + \frac{1}{4\varepsilon_1} \right)$; $C_{inj,D}$ and $C_{cha,D}$ could be determined by Eqs.

340 (B15) - (B16), and the detailed derivation of Eqs. (17) - (18) could be seen in Section S2 of *Supplementary Materials*.

Substituting Eq. (16) into the dispersivity coefficient (D_α), one has

$$D_\alpha = \alpha_2 |v_{a1}| + D_0 = \begin{cases} \frac{krQ}{2\pi r B \theta_{m1}} + D_0 = \frac{kQ}{2\pi B \theta_{m1}} + D_0, & r_s \leq r \leq r_0 \\ \frac{\alpha_0 Q}{2\pi r B \theta_{m2}} + D_0, & r > r_0 \end{cases}, \quad (19)$$

where D_0 is molecular diffusion coefficient [$L^2 T^{-1}$]. A few interesting features are notable here. First, because of the unique feature of a divergent flow field in which the velocity is inversely proportional to the radial distance, and the use of a dispersivity function that is proportional to the radial distance when $r \leq r_0$, the dispersion coefficient in Eq. (19) actually becomes constant. However, one must be aware that if other types of dispersivity equations are used (such as exponential and parabolic functions), the dispersion coefficient in Eq. (19) will depend on the radial distance from the well. Second, even when D_α becomes constant for a linear dispersivity function when $r \leq r_0$, the mechanical dispersion is still dominant, since the value of D_0 is generally much smaller than the mechanical dispersion term of $\frac{kQ}{2\pi B \theta_{m1}}$. For instance, the diffusion coefficient in water ranges from 1×10^{-9} to 2×10^{-9} m²/s, and it is much smaller in the porous media (Freeze and Cherry 1979). When $k = 0.01$, $Q = 0.1$ m³/s, $B=1$ m, $\theta_{m1} = 0.3$, one has $\frac{kQ}{2\pi B \theta_{m1}} = 5.3 \times 10^{-4}$ m²/s. Therefore, it is reasonable to ignore the molecular diffusion effect when $r \leq r_0$. The values of $\frac{kQ}{2\pi B \theta_{m1}}$ is dependent on k . The chosen value of $k = 0.01$ is

355

from experimental studies, for instance, $k = 0.018$ in Chen et al. (2007), and $k = 0.024$ and 0.013 in this study as shown in Table 5.

2.5. Extension of the new solution to a leaky-confined aquifer

Regardless of Eqs. (14) - (15) or Eqs. (17) - (18), the aquifer is assumed to be completely isolated from the underlying and overlying aquitards (strictly confined), which might not be true in real applications. As stated before (Zhan et al., 2009b; Zhan et al., 2009a), it is nearly impossible to maintain a strictly confined condition in terms of transport. That is because as long as solute in the aquifer is in contact with the upper or lower aquitard, molecular diffusion will always drive the solute from high concentration aquifer into the solute-free aquitard, even if the cross-formation flow in the aquitard does not exist. In fact, such diffusion-driven transport of solute into the aquitard and the subsequent back diffusion (from aquitard to aquifer when the aquifer solute concentration drops below the solute concentration in the aquitards) is responsible for many long tails in aquifer BTCs. The importance of aquitard in regulating solute transport has indeed been recognized by a number of investigators such as Chen (1985), Chen (1986), Yates (1988), Chen (1991), Novakowski (1992), Wang and Zhan (2013a), and Zhou et al. (2017).

In this section, the solutions of Eqs. (14) - (15) will be extended considering both underlying and overlying aquitards. The detailed derivation of the analytical solution in Laplace domain could be seen in Section S3 of *Supplementary Materials*.

In the aquifer, the solutions are

$$\bar{C}_{m1D} = T_1 \exp\left(\frac{r_D}{2\lambda}\right) A_i(\varphi_1) + T_2 \exp\left(\frac{r_D}{2}\right) B_i(\varphi_1), r_{wD} \leq r_D \leq r_{sD}, \quad (20a)$$

$$\bar{C}_{im1D} = \frac{\varepsilon_{im1}}{s + \varepsilon_{im1} + \mu_{im1D}} \bar{C}_{m1D}, r_{wD} \leq r_D \leq r_{sD}, \quad (20b)$$

$$\bar{C}_{m2D} = T_3 \exp\left(\frac{r_D}{2}\right) A_i(\varphi_2), r_D > r_{sD}, \quad (21a)$$

$$\bar{C}_{im2D} = \frac{\varepsilon_{im2}}{s + \varepsilon_{im2} + \mu_{im2D}} \bar{C}_{m2D}, r_D > r_{sD}; \quad (21b)$$

In the aquitards, the solutions are

$$380 \quad \bar{C}_{umD} = \bar{C}_{m1D} \exp(a_2 z_D - a_2), r_{wD} \leq r_D \leq r_{sD}, \quad (22a)$$

$$\bar{C}_{umD} = \bar{C}_{m2D} \exp(a_2 z_D - a_2), r_D > r_{sD}, \quad (22b)$$

$$\bar{C}_{uimD} = \frac{\varepsilon_{uim}}{s + \varepsilon_{uim} + \mu_{uimD}} \bar{C}_{umD}, r_D > r_{wD}, \quad (22c)$$

$$\bar{C}_{lmD} = \bar{C}_{m1D} \exp(b_1 z_D + b_1), r_{wD} \leq r_D \leq r_{sD}, \quad (23a)$$

$$\bar{C}_{lmD} = \bar{C}_{m2D} \exp(b_1 z_D + b_1), r_D > r_{sD}, \quad (23b)$$

$$385 \quad \bar{C}_{limD} = \frac{\varepsilon_{lim}}{s + \varepsilon_{lim} + \mu_{limD}} \bar{C}_{lmD}, r_D > r_{wD}, \quad (23c)$$

where letters “u” and “l” in the subscript represent the upper and lower aquitards, respectively; $\varphi_w =$

$$\left(\frac{E_3}{\lambda}\right)^{1/3} \left(r_{wD} + \frac{1}{4\lambda E_3}\right), \varphi_1 = \left(\frac{E_3}{\lambda}\right)^{1/3} \left(r_D + \frac{1}{4\lambda E_3}\right), \varphi_2 = E_4^{1/3} \left(r_D + \frac{1}{4E_4}\right); \varphi_{1s} = \left(\frac{E_3}{\lambda}\right)^{1/3} \left(r_{sD} + \frac{1}{4\lambda E_3}\right);$$

$$\varphi_{2s} = E_4^{1/3} \left(r_{sD} + \frac{1}{4E_4}\right); \text{ the expressions for } a_2, b_1, T_1, T_2 \text{ and } T_3 \text{ are listed in Table 4; } C_{inj,D} \text{ and } C_{cha,D}$$

could be determined by Eqs. (C36) - (C37), which can be seen in Section S3 of *Supplementary*

390 *Materials*.

The solutions of Chen (1985), Chen (1986), Yates (1988), and Chen (1991) are special cases of this study when $r_s \rightarrow \infty$, $t_{inj} \rightarrow \infty$, $\omega = 0$, and $V_{w,inj} = 0$. When $r_s \rightarrow \infty$, $t_{inj} \rightarrow \infty$, and $V_{w,inj} = 0$, the new solution reduces to the solution of Zhou et al. (2017). Novakowski (1992) considered the wellbore mixing effect in an aquifer-aquitard system, while he ignored other factors such as the skin effect, scale-
 395 dependent dispersivity, and mass transfer between the mobile and immobile domains in porous media.

3 Results and discussion

3.1 Test of new solutions

To test the new solution of this study, a numerical simulation based on the Galerkin finite-element method is conducted in the COMSOL Multiphysics platform. More details about the numerical
 400 simulation setup could be seen in Section S4 of *Supplementary Materials*. The parameters used in the numerical simulation are: $r_w = 2.5$ cm; $r_s = 12.5$ cm; $Q_{inj} = Q_{cha} = 100$ ml/s; $t_{inj} = 300$ s; $\alpha_1 = 2.5$ cm; $\alpha_2 = 2.5$ cm; $\theta_m = 0.30$; $\theta_{im} = 0.01$; $\omega = 0.001$ d⁻¹; $R_{m1} = R_{im1} = R_{m2} = R_{im2} = 1$; $B = 50$ cm; $\mu_{m1} = \mu_{m2} = \mu_{im1} = \mu_{im2} = 10^{-7}$ s⁻¹, and $h_{w,inj} = h_{w,cha} = B$. These parameters are from the experimental applications of Chao (1999), Chen et al. (2017), Wang et al. (2018) and Wang et al.
 405 (2020), in which Wang et al. (2020) summarized the values of reaction rate, retardation factor, dispersivity, porosity, and first-order mass transfer coefficient for sandy and clay used in numerous investigations, as shown in Table 4 of Wang et al. (2020). In addition, the values of retardation factor and reaction rate represent that the chemical reaction and sorption are weak for the tracer of KBr in the

experiment of Chao (1999). It is not surprising since KBr is commonly treated as a “conservative”
410 tracer.

As it is difficult to describe the wellbore mixing effect in COMSOL Multiphysics, the wellbore concentration is computed by the analytical solutions of Eqs. (14) - (15). Figures 1a and 1b show the comparison of concentration between the numerical and analytical solutions of this study, and good agreement between these two kinds of solutions is evident for different times and locations. The
415 comparisons between the numerical solution and analytical solutions of Eqs. (20) - (23) are shown in Section S4.2 of *Supplementary Materials*, and the agreement is also good between them.

3.2 Test of model using experimental data

To test the influence of the mixing effect, skin effect, scale effect and heterogeneity of the media on radial dispersion, the experimental data of Chao (1999) is employed. Chao (1999) reported a laboratory
420 experiment of radial dispersion in a sand tank with 244 cm in length, 122 cm in width and 6.35 cm in depth. A well with a radius of 1.0 cm fully penetrated a confined aquifer. Two observation wells were respectively located at 22.5 cm and 30.4 cm away from the well center. Potassium Bromide (KBr) is chosen as a conservative tracer. Before the tracer is introduced into the wellbore, a steady-state flow field is produced by injecting KBr-free water into the aquifer with a constant injection rate of 9.9
425 mL/min. The injection time is 5 hours ($t_{inj} = 300 \text{ min}$) for the tracer while maintaining the same injection rate of 9.9 mL/min. The experimental data of Chao (1999) was interpreted by Gao et al. (2009a) using the model of Chen et al. (2007), as shown in Figure 2. “SDM” and “CDM” in the legend of Figure 2 refer to the scale-dependent dispersivity model and the constant dispersivity model,

respectively. Chen et al. (2007) approximated the injection as an instantaneous source (the validity of
 430 such a treatment will be addressed later) and the mass M of the instantaneous injection is calculated by

$$M = C_0 Q_{inj} t_{inj}. \quad (24)$$

The other parameters of the analytical solution are listed in Table 5. The parameters estimated by Gao et al. (2009a) are also included in Table 5 for comparison. One may find that the goodness-of-fit between the observed data and models of Gao et al. (2009a) and Chen et al. (2007) seems good at the
 435 observation point close to the well, but they could not capture BTCs at $r=30.4$ cm. This is probably due to the following two reasons. Firstly, the model of Chen et al. (2007) used to best fit the data is an instantaneous slug test model, which is a rather gross approximation of the injection which lasted about 5 hours. A more proper way is to treat the 5 hours injection as a step source. Secondly, the solution of Chen et al. (2007) only considered the scale-dependent dispersivity, but ignored the mixing effect and
 440 the mass transfer between the mobile and immobile domains.

To test the new solutions of this study, we try to best fit the observed data again using the newly developed model considering the scale-dependent dispersivity, mixing effect and heterogeneity of the media (described using MIM). As there is no aquitard in the controlled laboratory experiment, the aquitard effect is irrelevant. Meanwhile, as there is no skin, so the skin effect is not included either. Best
 445 fitness between the analytical solution and the experimental data is an optimization process by minimizing the “error” between them,

$$E_{\text{error}} = \sum_{i=1}^N (C_{OBS} - C_{COM})^2, \quad (25)$$

where C_{OBS} and C_{COM} represent the observed and computed concentrations, respectively; Er is error; N is the number of sampling points. In this study, the genetic algorithm (GA) is employed to search the optimal parameter values, such as θ_{m2} , α_1 and ω_1 for CDM of Eqs. (14) - (15), and θ_{m2} , α_0 , k and ω_1 for ~~CDM~~ SDM of Eqs. (17) - (18). GA is a stochastic search method, based on natural selection, and it is preferred, due to its efficiency, simple programmability, and robustness. The GA could be implemented straightforwardly in MATLAB to facilitate computation (Katoch et al., 2020;Whitley, 1994;Deb et al., 2002). The estimated values of some key parameters are listed in Table 5. The errors between the observed and computed BTCs by different models are listed in Table 6. Figure 3 shows the fitness between the analytical solution and the experimental data, with and without scale-dependent dispersivity, respectively. As GA converges after 500 generations (iterations), the fitness is good as shown in Figure 3, and the estimated parameters are physically sound.

Comparing Figures 2 and 3 shows that the solutions of this study perform better than the model of Chen et al. (2007), since the fitness is good for both observation locations. To better evaluate the overall performance of the models for both locations, we have used Eq. (25) and the coefficient of determination (R^2) to compute the errors of best fitness with two BTCs simultaneously in Figures 2 and 3, and R^2 is defined by

$$R^2 = 1 - \frac{\sum_{i=1}^N (C_{OBS} - C_{COM})^2}{\sum_{i=1}^N (C_{OBS} - \bar{C}_{OBS})^2} \quad (26)$$

where \bar{C}_{OBS} is average concentration of observed data. The results are listed in the last two columns of Table 6. This table shows that the new model performs better. For example, when using CDM, the overall errors for best fitting two locations are 0.89 (which is the summation of 0.06 and 0.83 in Table 6)

for Chen et al. (2007), and 0.39 (which is the summation of 0.34 and 0.05 in Table 6) for this study. When using SDM, however, the overall errors for best fitting two locations are 0.78 for Chen et al. (2007), and 0.25 for this study. The overall R^2 shows the same observation as the overall E_r , where the overall R^2 is closer to 2, implying that the model precision is higher. Evidently, the model with scale effect is the best choice for interpreting the experimental data.

We have to emphasize that better fitting of one model than the other model with the experimental data should not be used as the only evidence of proof for model performance. That is because a model with more fitting parameters usually performs better than the model with less fitting parameters. Besides the best fitting exercises, however, one should pay more attention to see if the model adequately acknowledges the underlying physiochemical principles governing the transport processes. As far as we can see, the new model proposed in this study has honored the underlying physiochemical principles governing the radial dispersion process properly. In addition, the model performance (as reflected in the best fitting practice with the experimental data) is also considerably better. Therefore, on the basis of these two considerations, the new model of this study can be regarded as a significant advancement of present knowledge on radial dispersion. Furthermore, the new model is quite general and it encompasses almost all the existing models as subsets.

3.3 Sensitivity analysis

As the new model involves a number of controlling parameters, it is necessary to prioritize the importance of these parameters in terms of their control on the model performance. In this study, a

sensitivity analysis involving normalized parameters is conducted as follows (Kabala, 2001;Yang and Yeh, 2009)

$$SC_{i,j} = I_j \frac{\partial C_i}{\partial I_j}, \quad (2627)$$

490 where $SC_{i,j}$ is the sensitivity coefficient of the j^{th} parameter I_j at the i^{th} time; C_i is the concentration at the i^{th} time. I_j represents any one parameter of interest, like volume of water in the wellbore (V_w), k , $\theta_m = \theta_{m1} = \theta_{m2}$, $\omega = \omega_1 = \omega_2$, and so on. A larger $|SC_{i,j}|$ value means the higher sensitivity.

As the expression of the new analytical solution is complex, it is not easy to get the values of $SC_{i,j}$ directly from Eq. (2627). Therefore, a finite-difference scheme is used alternatively to approximate the
495 right-hand side term (Kabala, 2001;Yang and Yeh, 2009)

$$SC_{i,j} = I_j \frac{C_i(I_j + \Delta I_j) - C_i(I_j)}{\Delta I_j}, \quad (2728)$$

where ΔI_j is a small increment of I_j .

The main parameters of the new model include the volume of the water in the wellbore (V_w) for the mixing effect, r_s and α_s for the skin zone, θ_m and ω for the MIM model, and k for scale dependent
500 dispersivity. Figures 4a and 4b show $SC_{i,j}$ at $r=22.5$ cm and $r=30.4$ cm, respectively. The parameters used in these two figures are the same as those used in Figure 3.

Two observations could be found from Figures 4a and 4b. Firstly, the results are sensitive to the parameter of θ_m . To test such a finding, we use the model of this study (Eqs. (17) - (18)) with the mixing effect to best fit the experimental data of Chao (1999) (shown in Figure S54 in Section S5 of

505 *Supplementary Materials*), and the results show that the influence of the mixing effect could be negligible. Secondly, by comparing Figures 4a and 4b, we find that the sensitivity coefficient of V_w , r_s , α_s and $\alpha_s R$ on BTCs increases with the distance from the wellbore.

Figures 4a and 4b show that the sensitivity coefficient of V_w on BTCs is very small, which might contradict with the finding reported in some previous studies (Wang et al., 2018). A careful inspection
510 indicates that the well radius and the initial water level in the wellbore are very small in the experiment of Chao (1999), resulting in a very small value of V_w . From Eqs. (6) - (7), one can see that V_w could be influenced by the pumping rate, well radius, initial water level (h_0), and hydraulic parameters of the aquifer. In actual field practices, the value of V_w can be significantly larger than what is used in Chao (1999). Therefore, the sensitivity coefficient of V_w on BTCs will be investigated again using the well
515 radius and the initial water level that are more commonly seen in field applications, e.g., $r_w=5.0$ cm and $h_0=31.75$ cm, and the other parameters are the same as ones in Figure 3.

The sensitivity analysis after such modification shows that the parameter with the highest sensitivity coefficient is still θ_m , but the parameter with the second highest sensitivity coefficient becomes the volume of water in the wellbore (Figure 5). Figures 6 and 7 illustrate $SC_{i,j}$ of V_w for different r_w and
520 different observation locations, and that the sensitivity coefficient of V_w increases with the well radius, but decreases with the distance from the wellbore.

4 Conclusions

Radial dispersion is an important process in the fields of chemical engineering, environmental science, and hydrogeology. It has been commonly employed to describe the reactive transport in the subsurface, or to estimate aquifer transport parameters (dispersivity, porosity, and reactive rate, etc.) required in optimization of remediation strategies. However, previous studies did not include all of the mixing effect, skin effect, and mass transfer between the mobile and immobile domains in porous media.

In this study, a new general model is developed considering all above-mentioned factors. The new general model is against by a finite-element numerical model and existing experimental data. Meanwhile, the new model is also expanded considering the effect of the overlying and underlying aquitards and the scale-dependent dispersivity. The sensitivity analysis is conducted to prioritize influences of various controlling parameters on BTCs. The following conclusions could be summarized:

(1) The new general model honors the most relevant processes involved in radial dispersion (wellbore mixing effect, well skin effect, aquitard effect and mass transfer between the mobile and immobile domains), for which a solution has not yet been presented.

(2) The new general model fits the experimental data of Chao (1999) much better than previous models.

(3) The results are sensitive to parameters θ_m (mobile porosity) and V_w (the volume of water in the wellbore). When V_w is very small as in the laboratory experiment of Chao (1999), the sensitivity coefficient approaches 0. However, for typical values of V_w in actual field applications, the sensitivity coefficient of V_w increases significantly, and the value is often ranked as the second highest, after that of θ_m .

(4) The sensitivity coefficient of V_w increases with the well radius, while it decreases with increasing distance from the wellbore.

Data availability: The datasets used and/or analysed during the current study are available from the
545 corresponding author on reasonable request.

Author contributions: Methodology, derivation, code, and formal analysis, writing original draft: WS. Conceptualization, writing original draft, writing-review and editing, and supervision: QW. Vetting and technical support: HZ and RZ.

Competing interests: The contact author has declared that neither they nor their co-authors have any
550 competing interests.

Acknowledgments

This research was partially supported by Programs of the National Key Research and Development Program of China (No. 2021YFA0715900); National Natural Science Foundation of China (No.42222704 and No. 41972250); the Natural Science Foundation of Hubei Province (2021CFA089);
555 the Fundamental Research Funds for Central Universities, China University of Geosciences (Wuhan) (No. CUGGC07); the 111 Program (State Administration of Foreign Experts Affairs & the Ministry of Education of China, No. B18049); the Belt and Road Special Foundation of the State Key Laboratory of

Hydrology-Water Resources and Hydraulic Engineering(No. 2020492011), and Natural Science Foundation of Chongqing (cstc2020jcyj-msxmX1072).

560 **References**

Berkowitz, B., Scher, H., and Silliman, S. E.: Anomalous transport in laboratory-scale, heterogeneous porous media, *Water Resources Research*, 36, 149-158, <https://doi.org/10.1029/1999wr900295>, 2000.

Chao, H. C.: Scale dependence of transport parameters estimated from force-gradient tracer tests in heterogeneous formations, Ph.D, University of Colorado, Boulder, 1999.

Chen, C. S.: Analytical and approximate solutions to radial dispersion from an injection well to a geological unit with simultaneous diffusion into adjacent strata, *Water Resources Research*, 21(8), 1069-1076, <https://doi.org/10.1029/WR021i008p01069>, 1985.

Chen, C. S.: Solutions for radionuclide transport from an injection well into a single fracture in a porous formation, *Water resources research*, 22(4), 508-518, <https://doi.org/10.1029/WR022i004p00508>, 1986

Chen, C. S.: Semianalytical solutions for radial dispersion in a three - layer leaky aquifer system, *Groundwater*, 29(5), 663-670, <https://doi.org/10.1111/j.1745-6584.1991.tb00557.x>, 1991.

Chen, J.-S., Chen, C.-S., and Chen, C. Y.: Analysis of solute transport in a divergent flow tracer test with scale-dependent dispersion, *Hydrological Processes*, 21(18), 2526-2536, <https://doi.org/10.1002/hyp.6496>, 2007.

- Chen, J. S., Liu, Y. H., Liang, C. P., Liu, C. W., and Lin, C. W.: Exact analytical solutions for two-dimensional advection–dispersion equation in cylindrical coordinates subject to third-type inlet boundary condition, *Advances in Water Resources*, 34(3), 365-374,
580 <https://doi.org/10.1016/j.advwatres.2010.12.008>, 2011.
- Chen, K., Zhan, H., and Yang, Q.: Fractional models simulating Non - Fickian behavior in four - stage single - well push - pull tests, *Water Resources Research*, 53, 9528 - 9545,
<https://doi.org/10.1002/2017WR021411>, 2017.
- Chen, Y. J., Yeh, H. D., and Chang, K. J.: A mathematical solution and analysis of contaminant
585 transport in a radial two-zone confined aquifer, *Journal of contaminant hydrology*, 138-139, 75-82,
<https://doi.org/10.1016/j.jconhyd.2012.06.006>, 2012.
- Cihan, A., and Tyner, J. S.: 2-D radial analytical solutions for solute transport in a dual-porosity medium, *Water Resources Research*, 47(4), <https://doi.org/10.1029/2009wr008969>, 2011.
- Dagan, G.: Time-dependent macrodispersion for solute transport in anisotropic heterogeneous
590 aquifers, *Water Resources Research*, 24, 1491-1500, <https://doi.org/10.1029/WR024i009p01491>, 1988.
- Davis, M. E., and Davis, R. J.: *Fundamentals of Chemical Reaction Engineering*, 2002,
- De Hoog, F. R., Knight, J., and Stokes, A.: An improved method for numerical inversion of Laplace transforms, *SIAM Journal on Scientific and Statistical Computing*, 3, 357-366,
<https://doi.org/10.1137/0903022>, 1982.
- 595 Deb, K., Agrawal, S., Pratap, A., and Meyarivan, T.: A fast and elitist multiobjective genetic algorithm: NSGA-II, *IEEE Trans. Evol. Comput.*, 6, 182-197, <https://doi.org/10.1109/4235.996017>, 2002.

- Dentz, M., Kang, P. K., and Borgne, T. I.: Continuous time random walks for non-local radial solute transport, *Advances in Water Resources*, 82, 16-26, <https://doi.org/10.1016/j.advwatres.2015.04.005>, 2015.
- Di Dato, M., Fiori, A., de Barros, F. P., and Bellin, A.: Radial solute transport in highly heterogeneous aquifers: Modeling and experimental comparison, *Water Resources Research*, 53(7), 5725-5741, <https://doi.org/10.1002/2016WR020039>, 2017.
- Dubner, H., and Abate, J.: Numerical Inversion of Laplace Transforms by Relating Them to the Finite Fourier Cosine Transform, *Journal of the Acm*, 15, 115-123, <https://doi.org/10.1145/321439.321446>, 1968.
- Ederly, Y., Dror, I., Scher, H., and Berkowitz, B.: Anomalous reactive transport in porous media: Experiments and modeling, *Physical review. E, Statistical, nonlinear, and soft matter physics*, 91, 052130, <https://doi.org/10.1103/PhysRevE.91.052130>, 2015.
- Elenius, M. T., and Abriola, L. M.: Regressed models for multirate mass transfer in heterogeneous media, *Water Resources Research*, 55(11), 8646-8665, <https://doi.org/10.1029/2019wr025476>, 2019.
- Falade, G., and Brigham, W.: Analysis of radial transport of reactive tracer in porous media, *SPE reservoir engineering*, 4, 85-90, <https://doi.org/10.2118/16033-PA>, 1989.
- Gao, G., Zhan, H., Feng, S., Fu, B., Ma, Y., and Huang, G.: A new mobile-immobile model for reactive solute transport with scale-dependent dispersion, *Water Resources Research*, 46, 2010.
- Gao, G. Y., Feng, S. Y., Huo, Z. L., Zhan, H. B., and Huang, G. H.: Semi-analytical solution for solute radial transport dynamic model with scale-dependent dispersion, *Chinese Journal of Hydrodynamics*, 24, 156-163, 2009a.

Gao, G. Y., Feng, S. Y., Zhan, H. B., Huang, G. H., and Mao, X. M.: Evaluation of anomalous
620 solute transport in a large heterogeneous soil column with mobile-immobile model, *Journal of
Hydrologic Engineering*, 14, 966-974, [https://doi.org/10.1061/\(asce\)he.1943-5584.00000071](https://doi.org/10.1061/(asce)he.1943-5584.00000071), 2009b.

Gelhar, L. W., and Collins, M. A.: General analysis of longitudinal dispersion in nonuniform flow,
Water Resources Research, 7, 1511-1521, <https://doi.org/10.1029/WR007i006p01511>, 1971.

Gelhar, L. W., Welty, C., and Rehfeldt, K. R.: A critical review of data on field-scale dispersion in
625 aquifers, *Water Resources Research*, 28, 1955-1974, <https://doi.org/10.1029/92wr00607>, 1992.

Griffioen, J. W., Barry, D. A., and Parlange, J. Y.: Interpretation of two-region model parameters,
Water Resources Research, 34, 373-384, <https://doi.org/10.1029/97wr02027>, 1998.

Haddad, A. S., Hassanzadeh, H., Abedi, J., Chen, Z. X., and Ware, A.: Characterization of scale-
dependent dispersivity in fractured formations through a divergent flow tracer test, *Groundwater*, 53,
630 149-155, <https://doi.org/10.1111/gwat.12187>, 2015.

Haggerty, R., Fleming, S. W., Meigs, L. C., and McKenna, S. A.: Tracer tests in a fractured
dolomite: 2. Analysis of mass transfer in single - well injection - withdrawal tests, *Water Resources
Research*, 37, 1129 - 1142, <https://doi.org/10.1029/2000WR900334>, 2001.

Hansen, S. K., Berkowitz, B., Vesselinov, V. V., O'Malley, D., and Karra, S.: Push - pull tracer tests:
635 Their information content and use for characterizing non - Fickian, mobile - immobile behavior, *Water
Resources Research*, 52, 9565 - 9585, <https://doi.org/10.1002/2016WR018769>, 2016.

Hoopes, J. A., and Harleman, D. R.: Dispersion in radial flow from a recharge well, *Journal of
Geophysical Research*, 72, 3595-3607, <https://doi.org/10.1029/JZ072i014p03595>, 1967.

- Hsieh, P. A.: A new formula for the analytical solution of the radial dispersion problem, *Water Resources Research*, 22, 1597-1605, <https://doi.org/10.1029/WR022i011p01597>, 1986.
- Hsieh, P. F., and Yeh, H. D.: Semi-analytical and approximate solutions for contaminant transport from an injection well in a two-zone confined aquifer system, *Journal of Hydrology*, 519, <https://doi.org/10.1016/j.jhydrol.2014.08.046>, 2014.
- Huang, C. S., Tong, C., Hu, W., Yeh, H. D., and Yang, T.: Analysis of radially convergent tracer test in a two-zone confined aquifer with vertical dispersion effect: Asymmetrical and symmetrical transports, *Journal of hazardous materials*, 377, 8-16, <https://doi.org/10.1016/j.jhazmat.2019.05.042>, 2019.
- Huang, J., and Goltz, M. N.: Analytical solutions for solute transport in a spherically symmetric divergent flow field, *Transport in Porous Media*, 63, 305-321, <https://doi.org/10.1007/s11242-005-6761-4>, 2006.
- Kabala, Z. J.: Sensitivity analysis of a pumping test on a well with wellbore storage and skin, *Advances in Water Resources*, 24(5), 483-504, [https://doi.org/10.1016/s0309-1708\(00\)00051-8](https://doi.org/10.1016/s0309-1708(00)00051-8), 2001.
- Kang, P. K., Le Borgne, T., Dentz, M., Bour, O., and Juanes, R.: Impact of velocity correlation and distribution on transport in fractured media: Field evidence and theoretical model, *Water Resources Research*, 51, 940 - 959, <https://doi.org/10.1002/2014WR015799>, 2015.
- Katoch, S., Chauhan, S. S., and Kumar, V.: A review on genetic algorithm: past, present, and future, *Multimedia Tools and Applications*, 80, 8091 - 8126, <https://doi.org/10.1007/s11042-020-10139-6>, 2020.
- Le Borgne, T., and Gouze, P.: Non - Fickian dispersion in porous media: 2. Model validation from measurements at different scales, *Water Resources Research*, 44, W06427, <https://doi.org/10.1029/2007WR006279>, 2008.

660 Leitão, T. E., Lobo-ferreira, J. P., and Valocchi, A. J.: Application of a reactive transport model for
 interpreting non-conservative tracer experiments: The Rio Maior case-study, *Journal of Contaminant*
Hydrology, 24, 167-181, [https://doi.org/10.1016/S0169-7722\(96\)00008-3](https://doi.org/10.1016/S0169-7722(96)00008-3), 1996.

 Li, X. T., Wen, Z., Zhan, H., Zhan, H., and Zhu, Q.: Skin effect on single-well push-pull tests with
 the presence of regional groundwater flow, *Journal of Hydrology*, 577, 123931,
 665 <https://doi.org/10.1016/j.jhydrol.2019.123931>, 2019.

 Li, X. T., Wen, Z., Zhu, Q., and Jakada, H.: A mobile-immobile model for reactive solute transport
 in a radial two-zone confined aquifer, *Journal of Hydrology*, 580, 124347,
<https://doi.org/10.1016/j.jhydrol.2019.124347>, 2020.

 Lu, B., Zhang, Y., Zheng, C., Green, C. T., O'Neill, C., Sun, H.-G., and Qian, J.: Comparison of
 670 time nonlocal transport models for characterizing non-Fickian transport: From mathematical
 interpretation to laboratory application, *Water*, 10, <https://doi.org/10.3390/w10060778>, 2018.

 Moench, A., and Ogata, A.: A numerical inversion of the Laplace transform solution to radial
 dispersion in a porous medium, *Water Resources Research*, 17(1), 250-252,
<https://doi.org/10.1029/WR017i001p00250>, 1981.

675 Molinari, A., Pedretti, D., and Fallico, C.: Analysis of convergent flow tracer tests in a
 heterogeneous sandy box with connected gravel channels, *Water Resources Research*, 51(7), 5640-5657,
<https://doi.org/10.1002/2014wr016216>, 2015.

 Neuman, S. P., and Mishra, P. K.: Comments on “A revisit of drawdown behavior during pumping
 in unconfined aquifers” by D. Mao, L. Wan, T.-C. J. Yeh, C.-H. Lee, K.-C. Hsu, J.-C. Wen, and W. Lu,
 680 *Water Resources Research*, 48(2), W02801, <https://doi.org/10.1029/2011wr010785>, 2012.

Novakowski, K. S.: The analysis of tracer experiments conducted in divergent radial flow fields, Water resources research, 28(12), 3215-3225, <https://doi.org/10.1029/92WR01722>, 1992.

Philip, J.: Some exact solutions of convection - diffusion and diffusion equations, Water Resources Research, 30(12), 3545-3551, <https://doi.org/10.1029/94WR01329>, 1994.

685 Pickens, J. F., and Grisak, G. E.: Scale-dependent dispersion in a stratified granular aquifer, Water Resources Research, 17(4), 1191-1211, <https://doi.org/10.1029/WR017i004p01191>, 1981a.

Pickens, J. F., and Grisak, G. E.: Modeling of scale-dependent dispersion in hydrogeologic systems, Water Resources Research, 17(6), 1701-1711, <https://doi.org/10.1029/WR017i006p01701>, 1981b.

Reinhard, M., Shang, S., Kitanidis, P. K., Orwin, E., Hopkins, G. D., and Lebrón, C. A.: In Situ
690 BTEX Biotransformation under Enhanced Nitrate- and Sulfate-Reducing Conditions, Environmental Science & Technology, 31(1), 28-36, <https://doi.org/10.1021/es9509238>, 1997.

Schapery, R. A.: Approximate Methods of Transform Inversion for Viscoelastic Stress Analysis, 1962.

Shi, W., Wang, Q., and Zhan, H.: New simplified models of single - well push - pull tests with
695 mixing effect, Water Resources Research, 56(8), e2019WR026802, <https://doi.org/10.1029/2019WR026802>, 2020.

Silliman, S. E., and Simpson, E. S.: Laboratory evidence of the scale effect in dispersion of solutes in porous media, Water Resources Research, 23(8), 1667-1673, <https://doi.org/10.1029/WR023i008p01667>, 1987.

- 700 Soltanpour Moghadam, A., Arabameri, M., and Barfeie, M.: Numerical solution of space-time
variable fractional order advection-dispersion equation using radial basis functions, *Journal of
Mathematical Modeling*, 10(3), 549-562, <https://doi.org/10.22124/JMM.2022.21325.1868>, 2022.
- Stehfest, and Harald: Remark on algorithm 368: Numerical inversion of Laplace transforms,
Communications of the Acm, 13(10), 624, <https://doi.org/10.1145/355598.362787>, 1970.
- 705 Tang, D., and Babu, D.: Analytical solution of a velocity dependent dispersion problem, *Water
Resources Research*, 15(6), 1471-1478, <https://doi.org/10.1029/WR015i006p01471>, 1979.
- Tang, D., and Peaceman, D.: New analytical and numerical solutions for the radial convection-
dispersion problem, *SPE Reservoir Engineering*, 2(3), 343-359, <https://doi.org/10.2118/16001-PA>, 1987.
- van Genuchten, M. T., and Wierenga, P. J.: Mass transfer studies in sorbing porous media I.
710 analytical solutions¹, *Soil Science Society of America Journal*, 40(4), 473-480,
<https://doi.org/10.2136/sssaj1976.03615995004000040011x>, 1976.
- Veling, E.: Analytical solution and numerical evaluation of the radial symmetric convection-
diffusion equation with arbitrary initial and boundary data, *IAHS PUBLICATION*, 271-276, 2001.
- Veling, E. J. M.: Radial transport in a porous medium with Dirichlet, Neumann and Robin-type
715 inhomogeneous boundary values and general initial data: analytical solution and evaluation, *Journal of
Engineering Mathematics*, 75, 173-189, <https://doi.org/10.1007/s10665-011-9509-x>, 2011.
- Wang, Q., and Zhan, H.: Radial reactive solute transport in an aquifer–aquitard system, *Advances
in Water Resources*, 61, 51-61, <https://doi.org/10.1016/j.advwatres.2013.08.013>, 2013a.

- Wang, Q., and Zhan, H.: On different numerical inverse Laplace methods for solute transport
720 problems, *Advances in Water Resources*, 75, 80-92, <https://doi.org/10.1016/j.advwatres.2014.11.001>,
2015.
- Wang, Q., Shi, W., Zhan, H., Gu, H., and Chen, K.: Models of single-well push-pull test with
mixing effect in the wellbore, *Water Resources Research*, 54(12), 10155-10171,
<https://doi.org/10.1029/2018wr023317>, 2018.
- 725 Wang, Q., Gu, H., Zhan, H., Shi, W., and Zhou, R.: Mixing effect on reactive transport in a column
with scale dependent dispersion, *Journal of Hydrology*, 124494,
<https://doi.org/10.1016/j.jhydrol.2019.124494>, 2019.
- Wang, Q., Wang, J., Zhan, H., and Shi, W.: New model of reactive transport in a single-well push–
pull test with aquitard effect and wellbore storage, *Hydrology and Earth System Sciences*, 24, 3983-
730 4000, <https://doi.org/10.5194/hess-24-3983-2020>, 2020.
- Wang, Q. R., and Zhan, H. B.: Radial reactive solute transport in an aquifer-aquitard system,
Advances in Water Resources, 61, 51-61, <https://doi.org/10.1016/j.advwatres.2013.08.013>, 2013b.
- Webster, D. S., Procter, J. F., and Marine, J. W.: Two-well tracer test in fractured crystalline rock,
U.S. Geol. Surv., *Water Supply Paper*, 1544-1574, <https://doi.org/10.3133/wsp1544I>, 1970.
- 735 Whitley, L. D.: A genetic algorithm tutorial, *Statistics and Computing*, 4, 65-85,
<https://doi.org/10.1007/BF00175354>, 1994.
- Yang, S.-Y., and Yeh, H.-D.: Radial groundwater flow to a finite diameter well in a leaky confined
aquifer with a finite-thickness skin, *Hydrological Processes*, 23(23), 3382-3390,
<https://doi.org/10.1002/hyp.7449>, 2009.

740 Yates, S.: Three - dimensional radial dispersion in a variable velocity flow field, Water Resources Research, 24(7), 1083-1090, <https://doi.org/10.1029/WR024i007p01083>, 1988.

Yeh, H. D., and Chang, Y. C. i.: Recent advances in modeling of well hydraulics, Advances in Water Resources, 51, 27-51, <https://doi.org/10.1016/j.advwatres.2012.03.006>, 2013.

Zakian, V.: Numerical inversion of Laplace transform, Electronics Letters, 5, 120-121, 1969.

745 Zhan, H. B., Wen, Z., and Gao, G. Y.: An analytical solution of two-dimensional reactive solute transport in an aquifer–aquitard system, Water Resources Research, 45(10), W10501, <https://doi.org/10.1029/2008WR007479>, 2009a.

Zhan, H. B., Wen, Z., Huang, G. H., and Sun, D. M.: Analytical solution of two-dimensional solute transport in an aquifer–aquitard system, Journal of Contaminant Hydrology, 107(3-4), 162 - 174, <https://doi.org/10.1016/j.jconhyd.2009.04.010>, 2009b.

750 Zheng, C., and Wang, P. P.: MT3DMS: a modular three-dimensional multispecies transport model for simulation of advection, dispersion, and chemical reactions of contaminants in groundwater systems; documentation and user's guide, Alabama Univ University, 1999.

Zheng, L., Wang, L., and James, S. C.: When can the local advection–dispersion equation simulate non-Fickian transport through rough fractures?, Stochastic Environmental Research and Risk Assessment, 33, 931-938, <https://doi.org/10.1007/s00477-019-01661-7>, 2019.

Zhou, R., Zhan, H., and Chen, K.: Reactive solute transport in a filled single fracture-matrix system under unilateral and radial flows, Advances in Water Resources, 104, 183-194, <https://doi.org/10.1016/j.advwatres.2017.03.022>, 2017.

Nomenclature

Symbol	Description
$A_i(\cdot), B_i(\cdot)$	Airy functions of the first kind and the second kind, respectively
$A'_i(\cdot), B'_i(\cdot)$	Derivative of the Airy functions of the first kind and the second kind, respectively
α_0	Longitudinal dispersivity [L] in the formation zone at $r > r_0$
α_1, α_2	Longitudinal dispersivities [L] in the skin and formation zones, respectively
B	The thickness [L] of aquifer
b	The half of aquifer thickness [L]
C_{m1}, C_{im1}	Resident mobile and immobile concentrations [ML ⁻³] of the skin zone, respectively
C_{m2}, C_{im2}	Resident mobile and immobile concentrations [ML ⁻³] of the formation zone, respectively
C_{um}, C_{uim}	Resident mobile and immobile concentrations [ML ⁻³] of the upper aquitard, respectively
C_{lm}, C_{lim}	Resident mobile and immobile concentrations [ML ⁻³] of the lower aquitard, respectively
$C_{inj}(t), C_{cha}(t)$	Concentrations [ML ⁻³] of tracer in the wellbore at the injection and the chasing phases, respectively
C_0	Concentration [ML ⁻³] of tracer injected into the wellbore
C_w	Concentration [ML ⁻³] of tracer in the wellbore
D_u, D_l	Vertical dispersion coefficients [L ² T ⁻¹] of the upper and lower aquitards, respectively
D_0	Molecular diffusion coefficient [L ² T ⁻¹]
h	Hydraulic head [L]
h_0	Hydraulic head [L] at the r_e
$h_{w,inj}, h_{w,cha}$	Water level in the wellbore in the injection and chasing phases [L]
k	A constant [dimensionless] and ranges from 0 to 1
K_1, K_2	Hydraulic conductivities [LT ⁻¹] of skin and formation zones, respectively
K_d	Equilibrium distribution coefficient [M ⁻¹ L ³] for the linear sorption process
$I_m(\cdot), K_m(\cdot)$	The m^{th} -order modified Bessel function of the first and second kinds, respectively
Q	Pumping rate [L ³ T ⁻¹] (negative for injection and positive for pumping)
Q_{inj}, Q_{cha}	Well flow rates [L ³ T ⁻¹] in the injection and chasing phases, respectively.
r	Radial distance [L] from the center of the well

r_s	Distance [L] from the center of the well to the outer boundary of the skin zone
r_w	Radius [L] of the well
r_e	Radial distance [L] from the center of the well to the outer boundary
r_0	Radial distance [L] for the linear distance-dependent dispersivity
R_{m1}, R_{im1}	Retardation factors [dimensionless] for the mobile and immobile regions of the skin zone
R_{m2}, R_{im2}	Retardation factors [dimensionless] for the mobile and immobile regions of the formation zone
R_{um}, R_{uim}	Retardation factors [dimensionless] for the mobile and immobile regions of the upper aquitard
R_{lm}, R_{lim}	Retardation factors [dimensionless] for the mobile and immobile regions of the lower aquitard
t	Time [T]
t_{inj}, t_{cha}	Ending times [T] of the injection and the chasing phases, respectively
v_{a1}, v_{a2}	Average radial pore velocities [LT ⁻¹] of the skin zone, the formation zone, respectively
$v_{a1,inj}, v_{a1,cha}$	Average radial pore velocities [LT ⁻¹] at the well screen in the injection and chasing phases, respectively.
v_{um}, v_{lm}	Vertical velocities [LT ⁻¹] of the upper and lower aquitards, respectively
α_u, α_l	Dispersivities [L] of the upper aquitard and the lower aquitard, respectively
μ_{m1}, μ_{im1}	Decay constant for radioactive decay or reaction rate coefficient [T ⁻¹] in the mobile and immobile regions of the skin zone
μ_{m2}, μ_{im2}	Decay constant [T ⁻¹] for radioactive decay or reaction rate coefficient in the mobile and immobile regions of the formation zone
μ_{um}, μ_{uim}	Decay constant [T ⁻¹] for radioactive decay or reaction rate coefficient in the mobile and immobile regions of the upper aquitard
μ_{lm}, μ_{lim}	Decay constant [T ⁻¹] for radioactive decay or reaction rate coefficient in the mobile and immobile regions of the lower aquitard
$\theta_{m1}, \theta_{im1}$	Mobile and immobile porosities [dimensionless] in the skin zone
$\theta_{m2}, \theta_{im2}$	Mobile and immobile porosities [dimensionless] in the formation zone
$\theta_{um}, \theta_{uim}$	Mobile and immobile porosities [dimensionless] in the upper aquitard
$\theta_{lm}, \theta_{lim}$	Mobile and immobile porosities [dimensionless] in the lower aquitard
ρ_b	Bulk density [ML ⁻³] of the aquifer material
ω_1, ω_2	First-order mass transfer coefficients [T ⁻¹] in the skin and formation zones, respectively

s	Laplace transform variable with respect to the time t_D
Subscript	Description
D	Dimensionless form
m, im	Mobile and immobile regions, respectively
inj, cha	Injection and chasing phases, respectively
u, l	Upper and lower aquitard, respectively
1, 2	Parameters in the skin and formation regions, respectively
Acronyms	Description
ADE	Advection-dispersion equation
BTCs	The observed breakthrough curves
CDM	The constant dispersivity model
CTRW	Continuous-time random-walk models
fADE	Fractional-derivative ADE models
GA	The genetic algorithm
MFC	The mass flux continuity
MIM	Mobile-immobile model
MRMT	The multi-rate mass transfer model
RCC	The resident concentration continuity
SDM	The scale-dependent dispersivity model

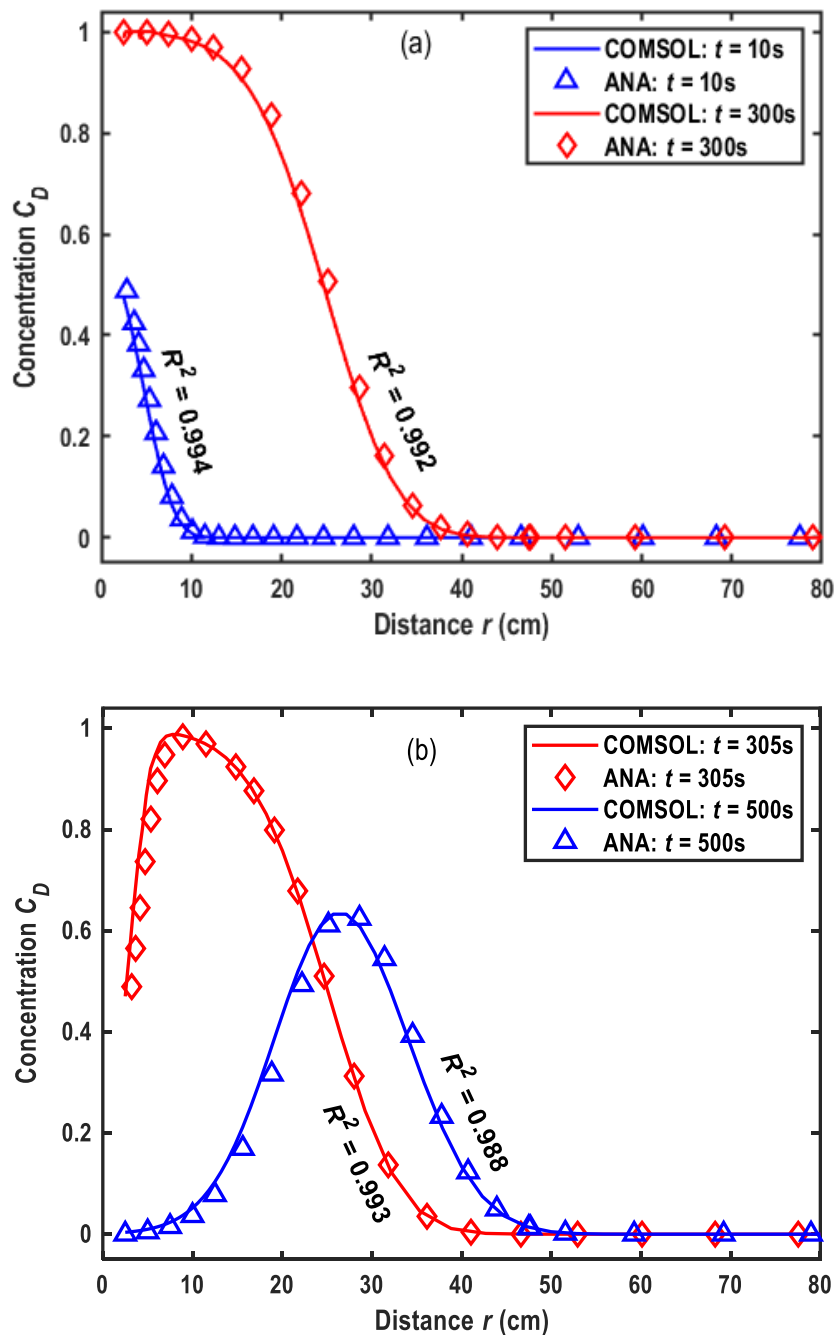


Figure 1. Comparison of the numerical solution by COMSOL Multiphysics and the analytical solution of this study for different times. (a). In the injection phase, (b). In the chasing phase.

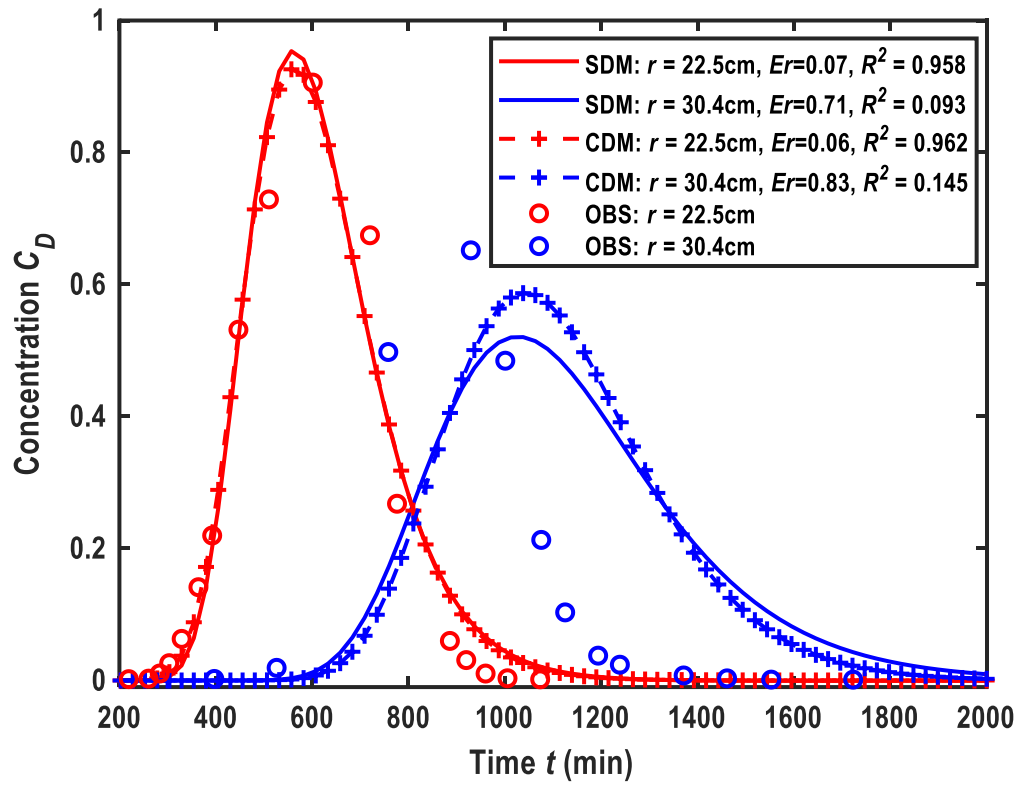


Figure 2. Fitness of observed BTC by the solution of Chen et al. (2007) which considers the scale effect but ignores the mixing and skin effects.

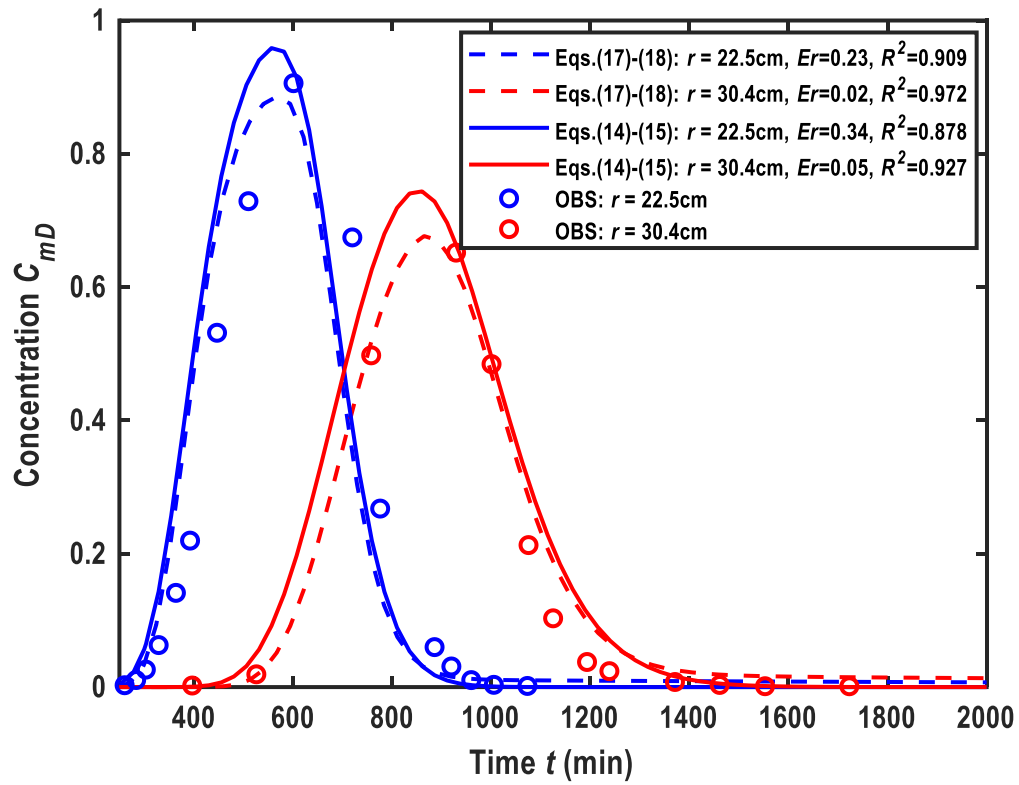
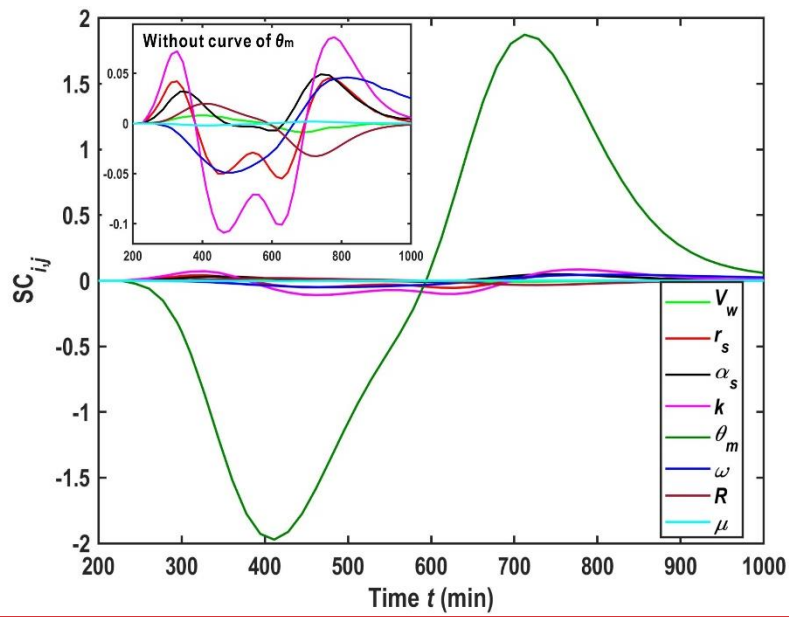
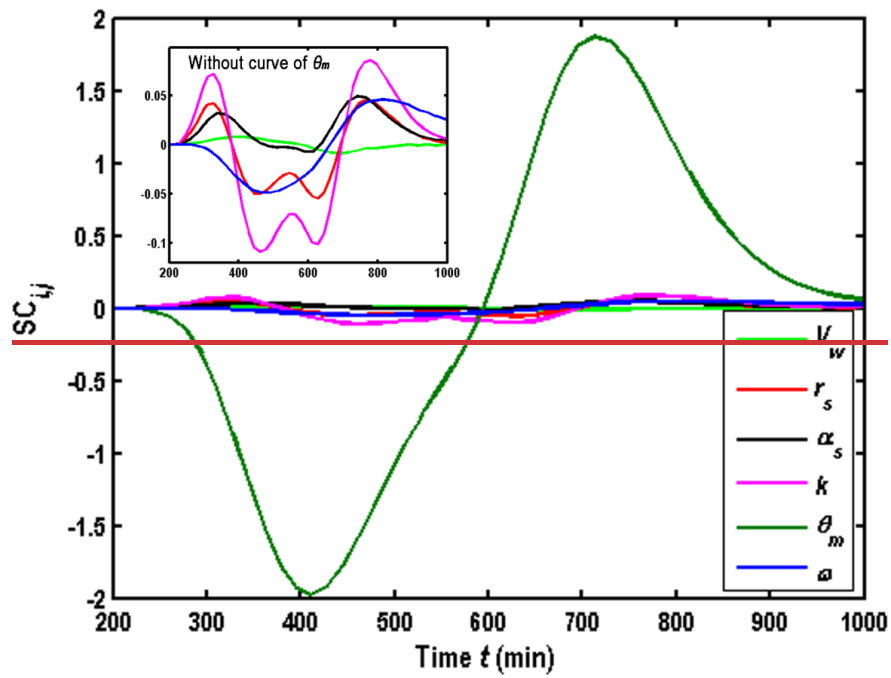
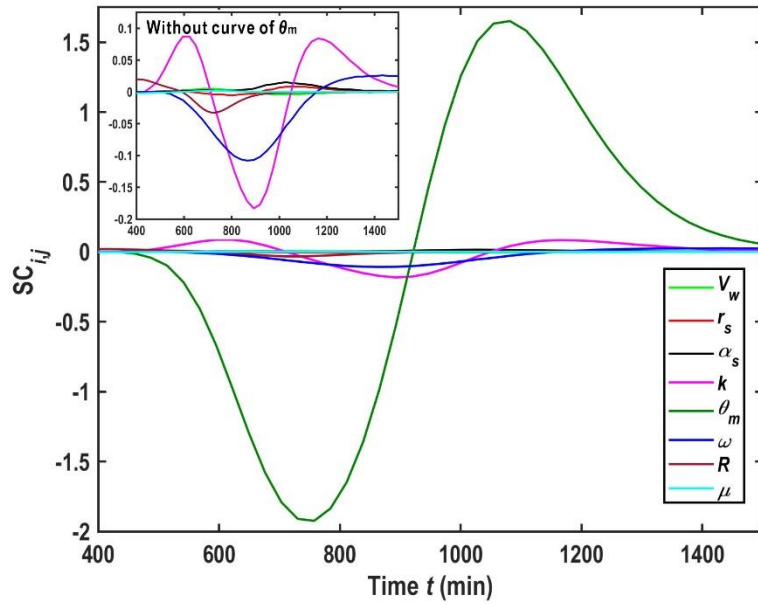
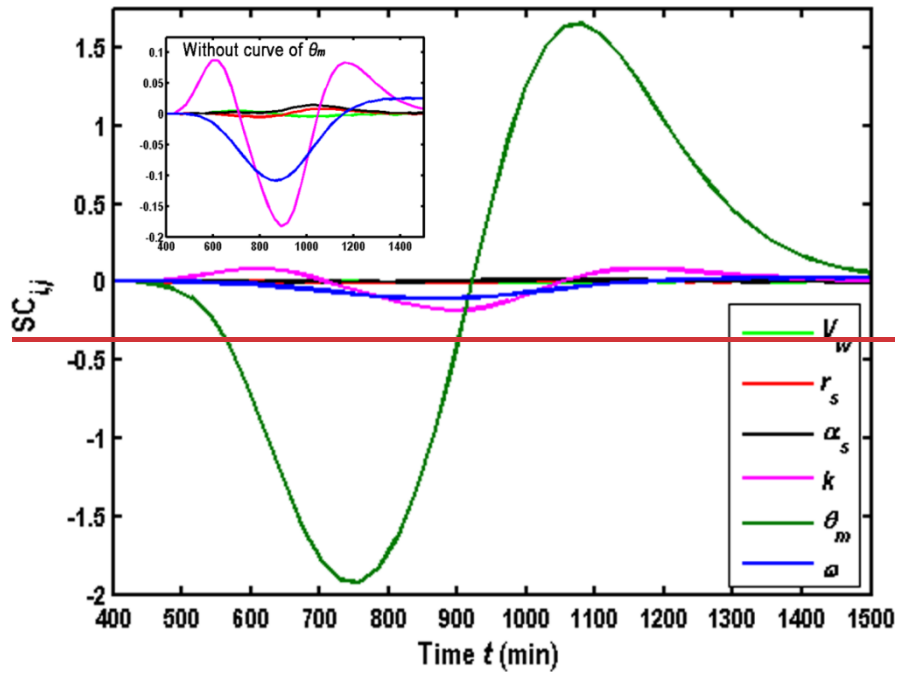


Figure 3. Fitness of observed BTC by new solutions of this study, where Eqs. (14) - (15): without scale effect and Eqs. (17) - (18): with scale effect, respectively.

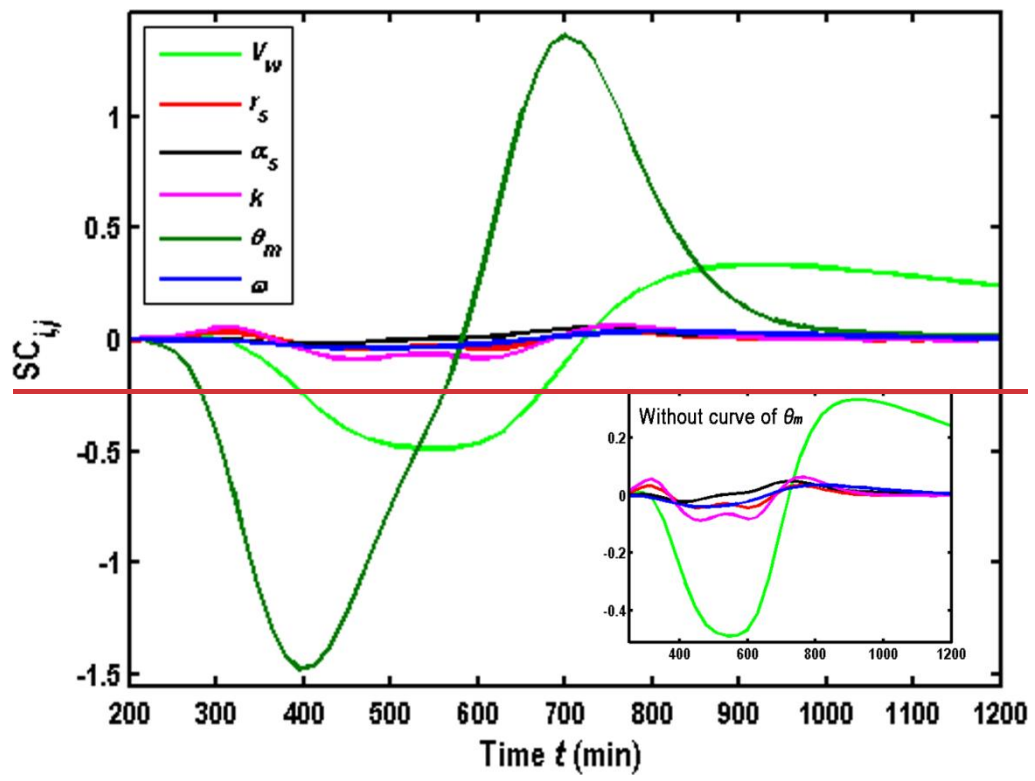


(a). $r=22.5$ cm



(b). $r=30.4$ cm

780 **Figure 4.** $SC_{i,j}$ of the parameters $r_w, r_s, k, \theta_m, \omega, R$ and μ using the parameters estimated by best fitting the experimental data. (a). $r=22.5$ cm, (b). $r=30.4$ cm.



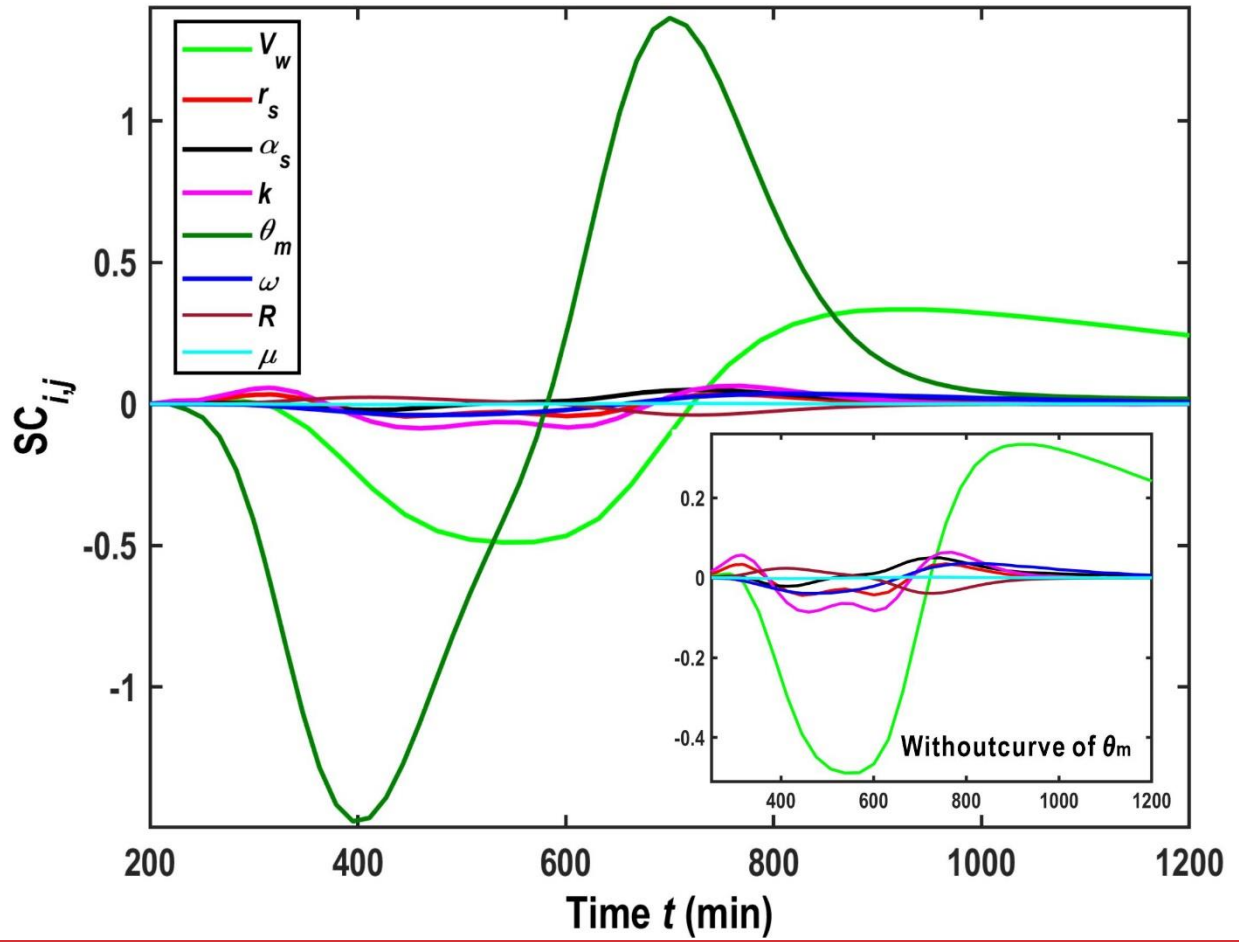


Figure 5. $SC_{i,j}$ of the parameters V_w , r_s , k , θ_m , ω , R and μ when increasing V_w .

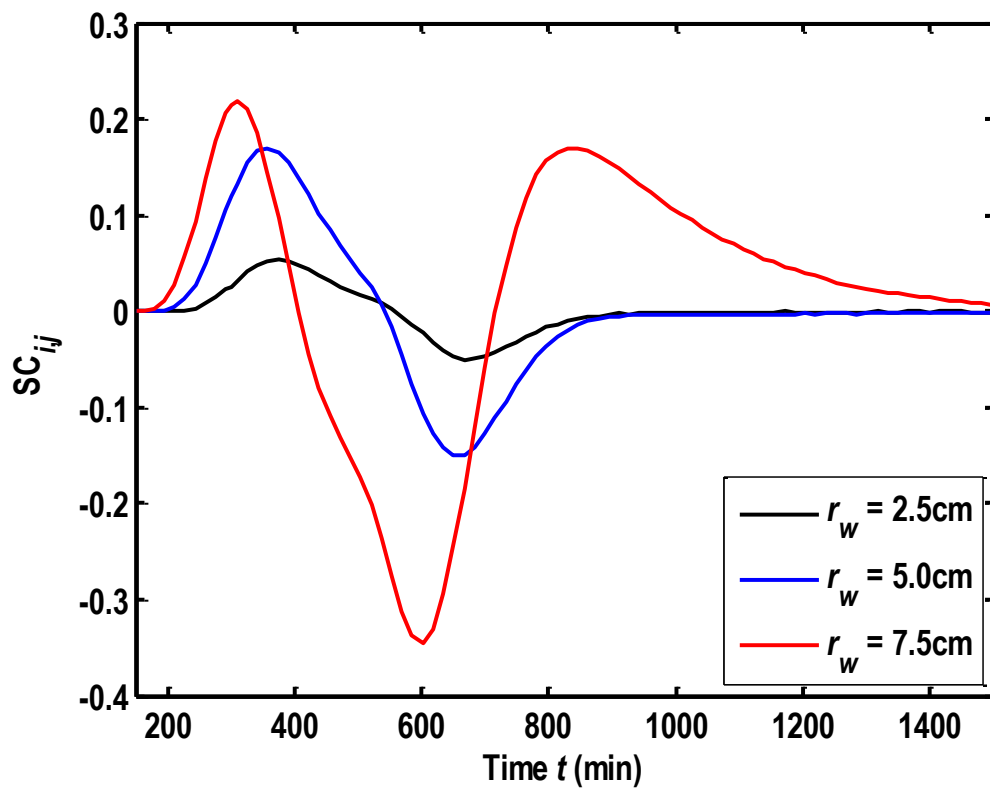


Figure 6. $SC_{i,j}$ of V_w for different r_w at $r=22.5$ cm.

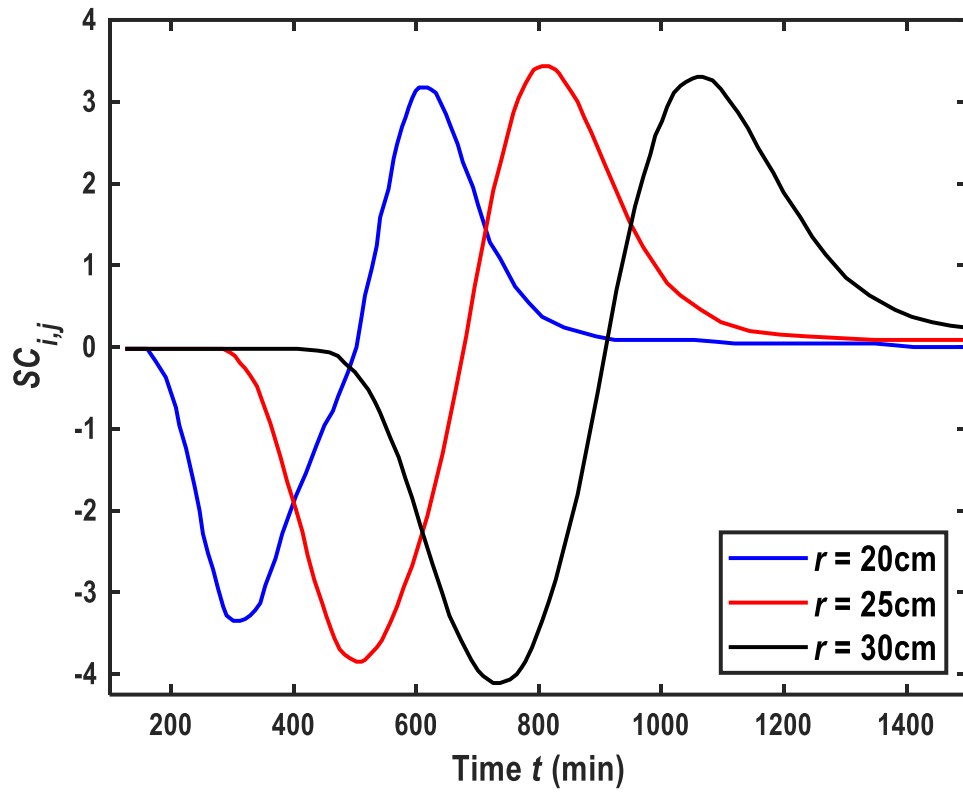


Figure 7. $SC_{i,j}$ of V_w for different observed locations when $r_w=5.0$ cm.

Table 1. Summary of the current models for the radial dispersion around the recharge well.

Authors	Conceptual models	GE	ME	SCE	SKE	Method
Hoopes and Harleman (1967)	Confined aquifer	ADE	N	N	N	Approximated solution and finite-difference solution
Gelbar and Collins (1971)	Confined aquifer	ADE	N	N	N	A boundary layer approximation
Tang and Babu (1979), Moench and Ogata (1981), Hsieh (1986), Tang and Peaceman (1987), Yates (1988), Cihan and Tyner (2011), Chen et al. (2012a)	Confined aquifer	ADE	N	N	N	Laplace transform
Chen (1985), Chen (1991)	Leaky-confined aquifer	ADE	N	N	N	Laplace transform
Chen (1986)	Fracture aquifer	ADE	N	N	N	Laplace transform
Falade and Brigham (1989)	Confined aquifer	MIM	N	N	N	Laplace transform
Novakowski (1992)	Leaky-confined aquifer	ADE	Y	N	N	Laplace transform
Philip (1994)	Confined aquifer	ADE	N	N	N	Finite-difference solution
Veling (2001), Veling (2011), Chen et al. (2011)	Confined aquifer	ADE	N	N	N	Generalized Hankel transform
Chen et al. (2007), Gao et al. (2009)	Confined aquifer	ADE	N	Y	N	Laplace transform
Chen et al. (2012b), Hsieh and Yeh (2014)	Confined aquifer	ADE	N	N	Y	Laplace transform
Wang and Zhan (2013)	Leaky-confined aquifer	ADE	N	N	N	Laplace transform
Zhou et al. (2017)	Fracture aquifer	MIM	N	N	N	Laplace transform
<u>Chen et al. (2017)</u>	<u>Confined aquifer</u>	<u>MIM</u>	<u>N</u>	<u>N</u>	<u>N</u>	<u>Laplace transform</u>
Wang et al. (2018)	Confined aquifer	ADE	Y	N	N	Laplace transform and Green's function method
<u>Huang et al. (2019)</u>	<u>Confined aquifer</u>	<u>ADE</u>	<u>N</u>	<u>N</u>	<u>Y</u>	<u>Laplace transform</u>
<u>Li et al. (2020)</u>	<u>Confined aquifer</u>	<u>MIM</u>	<u>N</u>	<u>N</u>	<u>Y</u>	<u>Laplace transform</u>
<u>Shi et al. (2020)</u>	<u>Confined aquifer</u>	<u>ADE</u>	<u>Y</u>	<u>N</u>	<u>N</u>	<u>Approximation</u>
<u>Wang et al. (2020)</u>	<u>Confined aquifer</u>	<u>MIM</u>	<u>Y</u>	<u>N</u>	<u>N</u>	<u>Laplace transform and Green's function method</u>

Note: “GE”, “ME”, “SCE”, and “SKE” represent governing equation, mixing effect, scale effect, and skin effect, respectively; “Y” and “N” represent whether the effect is considered or not.

795 **Table 2.** Expressions of coefficients in solutions of Eqs. (14a) - (15b)

N_1	$\frac{F - H_2 N_2}{H_1}$
N_2	$\frac{H_3 H_8 F - H_5 H_6 F}{H_1 H_5 H_7 + H_2 H_3 H_8 - H_2 H_5 H_6 - H_1 H_4 H_8}$
N_3	$\frac{H_3 F}{H_1 H_5} - \frac{H_2 H_3 N_2}{H_1 H_5} + \frac{H_4 N_2}{H_5}$
H_1	$\exp\left(\frac{r_{wD}}{2\lambda}\right) \left[\frac{1}{2} A_i(y_w) - \lambda \left(\frac{E_1}{\lambda}\right)^{1/3} A'_i(y_w) \right]$
H_2	$\exp\left(\frac{r_{wD}}{2\lambda}\right) \left[\frac{1}{2} B_i(y_w) - \lambda \left(\frac{E_1}{\lambda}\right)^{1/3} \exp\left(\frac{r_{wD}}{2}\right) B'_i(y_w) \right]$
H_3	$\exp\left(\frac{r_{sD}}{2\lambda}\right) A_i(y_{1s})$
H_4	$\exp\left(\frac{r_{sD}}{2\lambda}\right) B_i(y_{1s})$
H_5	$\exp\left(\frac{r_{sD}}{2}\right) A_i(y_{2s})$
H_6	$\exp\left(\frac{r_{sD}}{2\lambda}\right) \left[\frac{1}{2} A_i(y_{1s}) + \lambda \left(\frac{E_1}{\lambda}\right)^{1/3} A'_i(y_{1s}) \right]$
H_7	$\exp\left(\frac{r_{sD}}{2\lambda}\right) \left[\frac{1}{2} B_i(y_{1s}) + \lambda \left(\frac{E_1}{\lambda}\right)^{1/3} B'_i(y_{1s}) \right]$
H_8	$\exp\left(\frac{r_{sD}}{2}\right) \left[\frac{1}{2} A_i(y_{2s}) + (E_2)^{1/3} A'_i(y_{2s}) \right]$
F	$F = C_{inj,D} \frac{1 - \exp(-t_{inj,D} s)}{s} + C_{cha,D} \frac{\exp(-t_{inj,D} s)}{s}$

Table 3. Expressions of coefficients in solutions of Eqs. (17a) - (18c)

\mathcal{T}_1	$\frac{F - W_2 \mathcal{T}_2}{W_1}$
\mathcal{T}_2	$\frac{W_1 W_5}{W_1 W_4 - W_2 W_3} \mathcal{T}_3 + \frac{W_1 W_6}{W_1 W_4 - W_2 W_3} \mathcal{T}_4 - \frac{W_3 F}{W_1 W_4 - W_2 W_3}$
\mathcal{T}_3	$\frac{W_{13} W_{15} - W_{12} W_{16}}{W_{11} W_{16} - W_{13} W_{14}} \mathcal{T}_4$
\mathcal{T}_4	$\frac{W_3 F (W_1 W_8 - W_2 W_7) - W_7 F (W_1 W_4 - W_2 W_3)}{(W_1 W_5 \Theta + W_1 W_6) (W_1 W_8 - W_2 W_7) - (W_1 W_9 \Theta - W_1 W_{10}) (W_1 W_4 - W_2 W_3)}$
\mathcal{T}_5	$\frac{W_{14}}{W_{16}} \mathcal{T}_3 + \frac{W_{15}}{W_{16}} \mathcal{T}_4$
\mathcal{T}_6	0
Θ	$\frac{W_{13} W_{15} - W_{12} W_{16}}{W_{11} W_{16} - W_{13} W_{14}}$
W_1	$\exp\left(\frac{r_{wD}}{2\lambda}\right) \left[\frac{1}{2} A_i(y_w) - \lambda \left(\frac{E_1}{\lambda}\right)^{1/3} A'_i(y_w) \right]$
W_2	$\exp\left(\frac{r_{wD}}{2\lambda}\right) \left[\frac{1}{2} B_i(y_w) - \lambda \left(\frac{E_1}{\lambda}\right)^{1/3} \exp\left(\frac{r_{wD}}{2}\right) B'_i(y_w) \right]$
W_3	$\exp\left(\frac{r_{sD}}{2\lambda}\right) A_i(y_{1s})$
W_4	$\exp\left(\frac{r_{sD}}{2\lambda}\right) B_i(y_{1s})$
W_5	$r_{sD}^m K_m(\varepsilon_1 r_{sD})$
W_6	$r_D^m I_m(\varepsilon_1 r_D)$
W_7	$\exp\left(\frac{r_{sD}}{2\lambda}\right) \left[\frac{1}{2} A_i(y_{1s}) + \lambda \left(\frac{E_1}{\lambda}\right)^{1/3} A'_i(y_{1s}) \right]$
W_8	$\exp\left(\frac{r_{sD}}{2\lambda}\right) \left[\frac{1}{2} B_i(y_{1s}) + \lambda \left(\frac{E_1}{\lambda}\right)^{1/3} B'_i(y_{1s}) \right]$
W_9	$-k \varepsilon_1 r_{sD}^{m+1} K_{m-1}(\varepsilon_1 r_{sD})$
W_{10}	$k \{ m r_{sD}^{m-1} I_m(\varepsilon_1 r_D) + 0.5 \varepsilon_1 r_{sD}^m [I_{m-1}(\varepsilon_1 r_D) + I_{m+1}(\varepsilon_1 r_D)] \}$
W_{11}	$-k \varepsilon_1 r_{0D}^{m+2} K_{m-1}(\varepsilon_1 r_{0D})$
W_{12}	$k \{ m r_{0D}^m I_m(\varepsilon_1 r_{0D}) + 0.5 \varepsilon_1 r_{0D}^{m+1} [I_{m-1}(\varepsilon_1 r_{0D}) + I_{m+1}(\varepsilon_1 r_{0D})] \}$
W_{13}	$0.5 \exp\left(\frac{r_D}{2}\right) A_i(y_4) + \varepsilon_1^{1/3} \exp\left(\frac{r_D}{2}\right) A'_i(y_4)$

W_{14}	$r_{0D}^m K_m(\varepsilon_1 r_{0D})$
W_{15}	$r_{0D}^m I_m(\varepsilon_1 r_{0D})$
W_{16}	$\exp\left(\frac{r_{0D}}{2}\right) A_i(y_4)$

Table 4. Expressions of coefficients in solutions of Eqs. (20a) - (23c).

T_1	$\frac{F - G_2 T_2}{G_1}$
T_2	$\frac{G_3 G_8 F - G_5 G_6 F}{G_1 G_5 G_7 + G_2 G_3 G_8 - G_2 G_5 G_6 - G_1 G_4 G_8}$
T_3	$T_3 = \frac{G_3 F}{G_1 G_5} - \frac{G_2 G_3 T_2}{G_1 G_5} + \frac{G_4 T_2}{G_5}$
G_1	$\exp\left(\frac{r_{wD}}{2\lambda}\right) \left[\frac{1}{2} A_i(\varphi_w) - \lambda \left(\frac{E_3}{\lambda}\right)^{1/3} A'_i(\varphi_w) \right]$
G_2	$\exp\left(\frac{r_{wD}}{2\lambda}\right) \left[\frac{1}{2} B_i(\varphi_w) - \lambda \left(\frac{E_3}{\lambda}\right)^{1/3} B'_i(\varphi_w) \right]$
G_3	$\exp\left(\frac{r_{sD}}{2\lambda}\right) A_i(\varphi_{1s})$
G_4	$\exp\left(\frac{r_{sD}}{2\lambda}\right) B_i(\varphi_{1s})$
G_5	$\exp\left(\frac{r_{sD}}{2}\right) A_i(\varphi_{2s})$
G_6	$\exp\left(\frac{r_{sD}}{2\lambda}\right) \left[\frac{1}{2} A_i(\varphi_{1s}) + \lambda \left(\frac{E_3}{\lambda}\right)^{1/3} A'_i(\varphi_{1s}) \right]$
G_7	$\exp\left(\frac{r_{sD}}{2\lambda}\right) \left[\frac{1}{2} B_i(\varphi_{1s}) + \lambda \left(\frac{E_3}{\lambda}\right)^{1/3} B'_i(\varphi_{1s}) \right]$
G_8	$\exp\left(\frac{r_{sD}}{2}\right) \left[\frac{1}{2} A_i(\varphi_{2s}) + E_4^{1/3} A'_i(\varphi_{2s}) \right]$
F	$C_{inj,D} \frac{1 - \exp(-t_{inj,D} s)}{s} + C_{cha,D} \frac{\exp(-t_{inj,D} s)}{s}$
E_3	$s + \varepsilon_{m1} + \mu_{m1D} - \frac{\varepsilon_{m1} \varepsilon_{im1}}{s + \mu_{im1D} + \varepsilon_{im1}} - \frac{a_2 \theta_{um} \alpha_2^2 D_u}{2A \theta_{m1} b^2} + \frac{b_1 \theta_{lm} \alpha_2^2 D_l}{2Ab^2 \theta_{m1}}$
E_4	$\frac{1}{\eta} \left(s + \varepsilon_{m2} + \mu_{m2D} - \frac{\varepsilon_{m2} \varepsilon_{im2}}{s + \mu_{im2D} + \varepsilon_{im2}} - \frac{a_2 \theta_{um} \alpha_2^2 D_u}{2A \theta_{m2} b^2} + \frac{b_1 \theta_{lm} \alpha_2^2 D_l}{2Ab^2 \theta_{m2}} \right)$
a_2	$-\sqrt{s + \varepsilon_{um} + \mu_{umD} - \frac{\varepsilon_{um} \varepsilon_{uim}}{s + \mu_{uimD} + \varepsilon_{uim}}}$
b_1	$\sqrt{s + \varepsilon_{lm} + \mu_{lmD} - \frac{\varepsilon_{lm} \varepsilon_{lim}}{s + \mu_{limD} + \varepsilon_{lim}}}$

Table 5. Parameter values used in Figures 2 and 3

Parameters	SDM of Chen (2007)	CDM of Chen (2007)	Eqs. (17) - (18)	Eqs. (14) - (15)
θ (-)	0.58	0.58	\	\
$\theta_{m1} = \theta_{m2}$ (-)	\	\	0.38	0.39
$\theta_{im1} = \theta_{im2}$ (-)	\	\	0.04	0.02
$\alpha_1 = \alpha_2$ (cm)	\	0.45	0.50	0.45
k (-)	2.4×10^{-2}	\	1.3×10^{-2}	\
r_0 (cm)	\	\	10000	\
α_0 (cm)	\	\	0.50	\
$\omega_1 = \omega_2$ (d ⁻¹)	\	\	1.0×10^{-3}	1.0×10^{-3}
t_{inj} (<u>min</u>)	<u>↓</u>	<u>↓</u>	<u>300</u>	<u>300</u>
μ_{m1} (s ⁻¹)	0.0	0.0	1.0×10^{-7}	1.0×10^{-7}
μ_{m2} (s ⁻¹)	0.0	0.0	1.0×10^{-7}	1.0×10^{-7}
μ_{im1} (s ⁻¹)	0.0	0.0	1.0×10^{-7}	1.0×10^{-7}
μ_{im2} (s ⁻¹)	0.0	0.0	1.0×10^{-7}	1.0×10^{-7}
$h_{w,inj}$ (cm)	\	\	6.35	6.35
$h_{w,cha}$ (cm)	\	\	6.35	6.35
r_s (cm)	\	\	r_w	r_w
$R = R_{m1} = R_{im1} = R_{m2} = R_{im2}$ (-)	1			

Note: “SDM” represents the scale-dependent dispersivity model; “CDM” represents the constant dispersivity model; “-” represents that the variable is dimensionless; “\” represents that the variable is not included in the model.

Table 6. Errors between observed and computed BTCs in Figures 2 and 3.

Models	Solutions	Observation location (cm)	Error (E_r)		R^2	
CDM	Chen et al. (2007)	22.5	0.06	0.89	<u>0.962</u>	<u>1.107</u>
		30.4	0.83		<u>0.145</u>	
	This study	22.5	0.34	0.39	<u>0.878</u>	<u>1.805</u>
		30.4	0.05		<u>0.927</u>	
SDM	Chen et al. (2007)	22.5	0.07	0.78	<u>0.958</u>	<u>1.051</u>
		30.4	0.71		<u>0.093</u>	
	This study	22.5	0.23	0.25	<u>0.909</u>	<u>1.881</u>
		30.4	0.02		<u>0.972</u>	